Treatment Planning Adaptions for Hypoxia in Proton Therapy for Head and Neck Cancer

Amalie Storesund

Master thesis in Medical Physics

Department of Physics and Technology

University of Bergen

June 2022

Supervisors: Kristian Smeland Ytre-Hauge and Sara Pilskog

Acknowledgements

I would like to thank my supervisors associate professor Kristian Smeland Ytre-Hauge and associate professor Sara Pilskog for giving me the opportunity to work on this fascinating thesis. Without your support and guidance, it would not have been possible. I would furthermore like to thank PhD candidate Helge Henjum, I could always count on you to answer my many questions and fixing countless technical issues. I would like to thank Dr. Bjarne Christian Hagen for reading through my thesis and giving invaluable feedback, even though it was Greek to him. Lastly, I would like to thank my partner Tor Gunnar Hagen, for being my rock, always supporting me through my ups and down, and telling me innumerable silly jokes.

Amalie Storesund

Bergen, June 2022

Abstract

Aim: Perform treatment planning adaptations for proton therapy to correct for hypoxia in head and neck cancer (HNC).

Material and methods: Hypoxic subvolumes were defined using three pO_2 (oxygen partial pressure) thresholds, 5 mmHg, 7.5 mmHg and 10 mmHg, using [^{18}F]EF5 PET/CT images for a HNC patient. FLUKA Monte Carlo simulations were then performed to calculate the oxygen enhancement ratio (OER) and relative biological effectiveness (RBE) weighted dose. Three additional treatment plans were made, one for each pO_2 threshold, before OER adapting the dose objectives for the hypoxic subvolumes using Eclipse treatment planning system.

Results: the method successfully defined and increased the biological dose for three pO_2 threshold defined hypoxic regions. However, the dose to the surrounding normoxic tumour tissue was also increased.

Contents

List of abbreviations

ASCII	American Standard Code for Information Interchange
CT	Computed Tomography
CTV	Clinical Target Volume
DCE	Dynamic-Contrast-Enhanced
DVH	Dose Volume Histogram
FLAIR	FLUKA Advanced Interface
GTV	Gross tumour Target Volume
HTV	Hypoxic Target Volume
IMPT	Intensity Modulated Proton Therapy
IMRT	Intensity Modulated Radiation Therapy
LET	Linear Energy Transfer
LETd	Dose averaged Linear Energy Transfer
LQ	Linear-Quadratic
MRI	Magnetic Resonance Imaging
OAR	Organs At Risk
OER	Oxygen Enhancement Ratio
PET	Positron Emission Tomography
PO_2	Oxygen Partial Pressure
PTV	Planning Target Volume
QUANTEC	Quantitative Analysis of Normal Tissue Effects
RBE	Relative Biological Effectiveness
ROWD	RBE and OER Weighted Dose
SOBP	Spread Out Bragg Peak
SUV	Standard Uptake Value
TCP	Tumour Control Probability

1. Introduction

1.1 Proton therapy

Cancer is commonly treated using chemotherapy, surgery, ionizing radiation or a combination of treatments. The treatment is determined by several factors such as the type and stage of cancer [1]. Ionizing radiation include photons as well as ions and is used to kill cancer cells by destroying the DNA. The use of protons for cancer treatment was first proposed by Robert Wilson in 1946, with the first proton treatment in 1955 at the Lawrence Berkley Laboratory [2]. Protons centres are now spread all over the world with increasing amounts of countries investing in proton therapy. The use of photons is well established in Norway, whereas the first proton centres are under construction.

With protons better dose conformity can be achieved due to the narrow Bragg peak [3], as seen in figure 1.1. This allows for irradiation of difficult tumour sites, such as the brain, eye and spinal cord, and more importantly reduce the tissue volume being exposed to radiation.

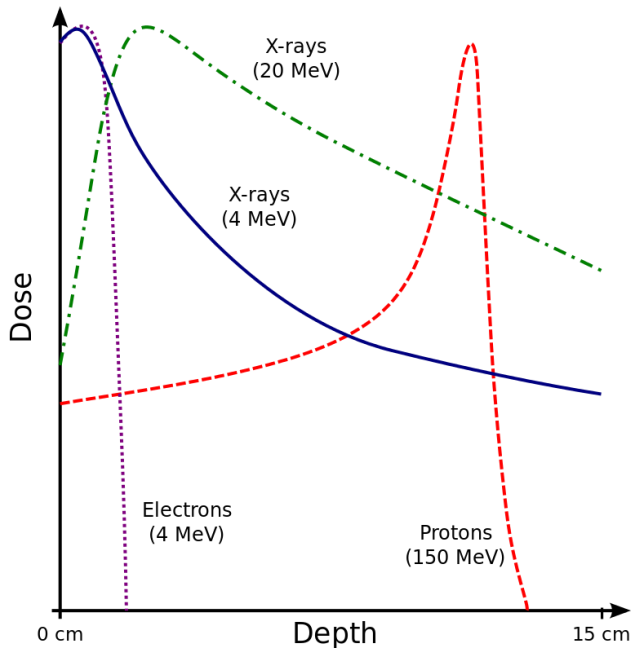

Figure 1.1: Comparison of different dose depth curves for photons (green and blue), electrons (purple) and protons (red). The Bragg peak for protons is deeper in tissue and narrower compared to photons. [4].

Compared to photons, protons have increased linear energy transfer (LET) which is the average energy deposited per unit length as an ionizing particle passes through a medium. The relative biological effectiveness (RBE), the ratio of dose needed to produce the same biological effect for one type of radiation compared to another, is also increased. Typically, a constant RBE of 1.1 is used for protons clinically, however there exist several different variable RBE models. One of which is the Rørvik weighted RBE model [5] which will be used in this thesis alongside a RBE of 1.1.

Protons therefore have several advantages over photons when trying to overcome the radioresistance caused by hypoxia.

1.2 Hypoxia; challenges and uses clinically

Cancer tissue is described as hypoxic when it has a low amount of oxygen, usually defined by having a pO_2 (oxygen partial pressure) lower than 8-10 mmHg (=133.322 Pa) [6]. pO_2 reflects the relationship between oxygen consumption and delivery in tissue [7]. Normoxic tissue on the other hand is well oxygenated tissue and has a pO_2 up to 100 mmHg.

It is well documented that hypoxic tumours pose a challenge in radiation therapy. Hypoxia increases the radioresistance leading to poorer overall survival for many patients with solid tumours independently of treatment [3]. Moreover, distant metastatic spread is also increased regardless of initial treatment [8]. Furthermore, the decreased DNA repair and resistance to apoptosis can give rise to genetic instabilities. Radiation with protons unlike photons reduces the effects of hypoxia as the increased LET for protons reduces the oxygen enhancement ratio (OER). OER is the ratio of dose needed to produce the same damage in hypoxic versus normoxic tissue. Due to the narrow Bragg peak of protons, it easier to tailor the dose distribution adapting for hypoxic regions. This makes proton therapy a prime tool to combat the effects of hypoxia.

To overcome the increased radioresistance of hypoxia different methods have been proposed. Some of which include dose painting, LET painting and RBE and OER weighted dose.

Dose painting involves prescribing a heterogenous dose to the tumour volume based on a dose modification factor [3, 9]. This dose modification is typically derived from the uptake or signal for the imaging method used. This can be done by splitting the PTV (planning target volume) into hypoxic and normoxic tissue, dose painting by contours, or dividing the PTV into voxels with individually estimated radioresistance, dose painting by numbers.

LET painting is a similar concept as dose painting only adjusting the LET instead. This is done by redistributing the LET [3]. The high LET values are targeted at the hypoxic volume, lowering the OER in the region, while lower LET values are targeted at the normoxic tissue. There are also studies looking into a combination of dose and LET painting.

Lastly RBE and OER weighted dose are being studied. Here in addition to OER adjusting the dose, the RBE for protons is also included in the calculations [6].

There are several clinical trials looking into dose painting by numbers or contours using photons [10-15]. None of the trials directly connects pO_2 to the signal in the images acquired. The hypoxic volume is for example instead defined by a threshold value of 50% of the uptake or signal intensity in the images or not derived from oxygen levels in the tumour [12-14]. The dose escalation in the included trials is either based on a constant 10% increase of prescribed dose [10] or determined by different image intensity and dose parameters [11-14] . In conclusion no clinical trials were found were the hypoxic volume or voxels are directly defined by the pO_2 or where OER was used in calculating the dose modifier. Furthermore, no published clinical trials of adapting the radiation to combat hypoxia for proton therapy could be found.

Apart from the methods discussed here there is also ongoing research into hypoxia imaging and different drugs to combat the effects of hypoxia.

1.3 Project objectives and motivation

The aim of this thesis is to perform treatment planning adaptations to correct for hypoxia in head and neck cancer (HNC). The motivation for this is to see what results can be achieved by dose escalation based on OER including two RBE models for proton therapy. One

challenge in dose planning is to determine the threshold for hypoxic versus normoxic tissue. Several pO_2 thresholds were therefore tested to define the hypoxic regions, giving different treatment plans and biological dose distributions.

The research questions for this thesis are to:

- Define hypoxic subvolumes for a HNC patient using multiple pO_2 thresholds for hypoxia
- Create proton treatment plans for the different subvolumes and adapt for hypoxia using OER and RBE
- Evaluate the strengths and weaknesses of choosing different pO_2 thresholds for the hypoxic subvolume
- Create a process that can be implemented clinically

2. Physics of particle therapy

2.1 Proton interactions with matter

The most important interactions for proton therapy are non-elastic nuclear reactions, inelastic and elastic Coulomb scattering (figure 2.1).

Elastic Coulomb scattering is when a proton comes close to the nucleus (see figure 2.1b) [16]. The nucleus will have a larger mass compared to the proton and the repulsive coulomb force will deflect it. This will not lead to any energy loss, however the proton will no longer be traveling in a straight line, rather at an angle from the original direction. This can lead to the proton beam spreading outwards.

There is also inelastic Coulomb scattering, which is when the proton collides with an orbital electron (see figure 2.1a). The proton will then transfer some of its energy to the electron either exciting or ionizing the electron. However, the path of the proton remains unchanged due to the low mass of the electron compared to the proton. This type of scattering leads to an approximately continuous loss of kinetic energy [16].

Lastly there are non-elastic nuclear reactions. These are less frequent than the other interactions but has a larger effect on the energy loss. Non-elastic nuclear reactions are when the proton collides with the nucleus, knocking out protons, neutrons or light nucleon clusters (see figure 2.1c). These particles will have much lower energy and larger angles than the original proton. Furthermore, the nucleus is left in an excited state, leading to the emission of photons [16].

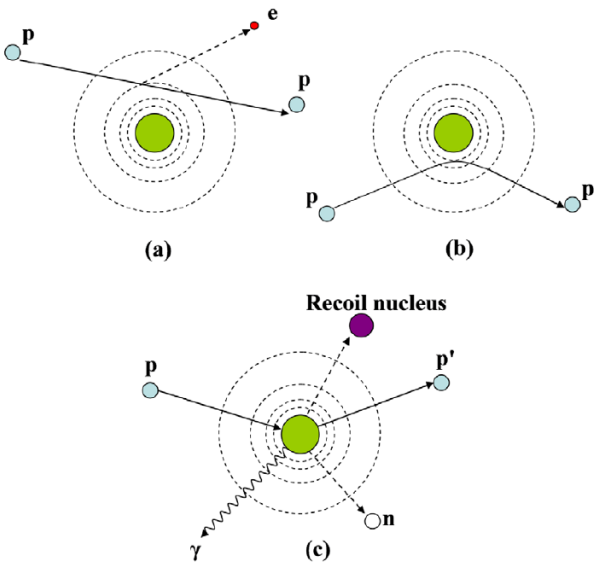

Figure 2.1: The different proton interactions where p is proton, e is an electron, n is a neutron and ϒ is a photon. a) inelastic Coulomb scattering b) elastic Coulomb scattering and c) non-elastic nuclear interaction [16].

2.1.1 Energy loss of protons

Linear energy transfer (LET) is the linear stopping power which is the average energy loss per unit length as an ionizing particle passes through a medium. LET is given in equation 2.1 [2].

$$LET = -\frac{dE}{dx} \tag{2.1}$$

Where *-dE* is the energy loss over distance *dx* and is typically expressed in keV/µm. LET is closely related to the biological effectiveness of radiation and dose [2].

The energy loss of a heavier charged particle, such as protons, due to ionization and excitation caused by inelastic Coulomb scattering and non-elastic nuclear reactions, can be described by the Bethe Bloch equation (eq. 2.2) [17].

$$-\frac{dE}{dx} = \frac{4\pi n z^2 Z^2 e^4}{m_e v^2}\left[ln\frac{2m_e v^2}{I\left[1-\left(\frac{v}{c}\right)^2\right]} - \left(\frac{v}{c}\right)^2\right] \tag{2.2}$$

Where n is the number of electrons per cm^3, z the charge of the particle, Z is the atomic number, e is the elementary charge, m_e the electronic mass, , v the velocity, I is the mean

excitation potential and c is the speed of light. The equation is valid for energies above 0.5 MeV [18] and depend on the charge and velocity of the traversing particle. For a proton with energy below 1 GeV the equation is proportional to $1/v^2$ [17]. This means that as the particle slows down, the energy loss will increase and in turn increasing the LET and dose. This leads to maximum energy loss near the end of the particles range. This is called the Bragg peak and can be seen in figure 2.2. The large deposition of energy followed by a sharp decrease makes protons and other heavier charged particles ideal candidates in radiation therapy. This is because one can concentrate the dose inside the target volume and minimize the dose to surrounding normal tissues.

The target volume is rarely the width of a Bragg peak from a monoenergetic beam. However, by using several beams with slightly different energies, one can achieve a spread-out Bragg peak (SOBP). This can be manipulated to cover the width of the target volume.

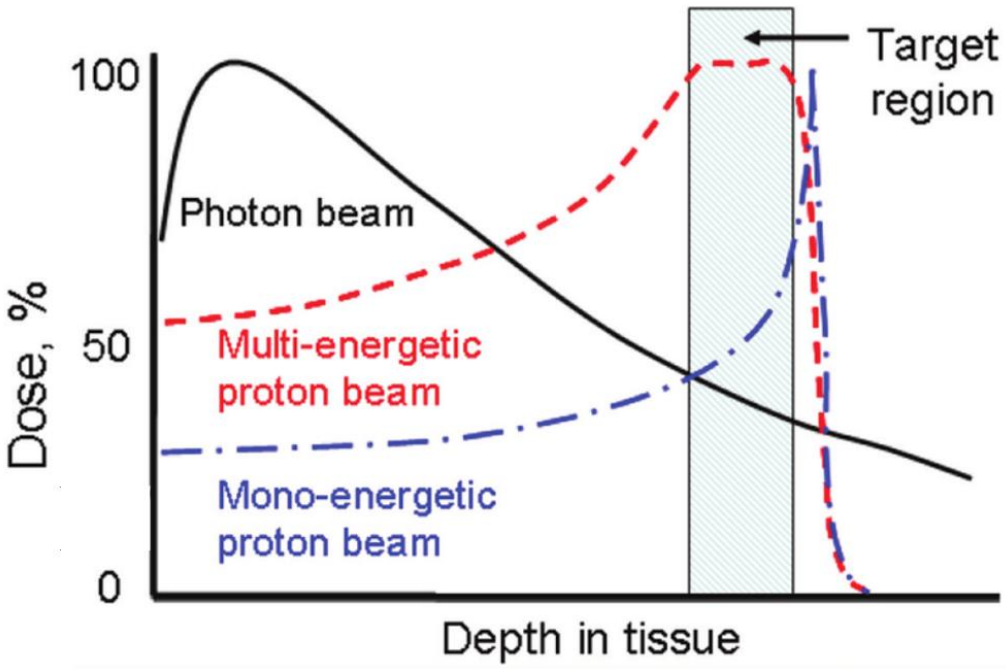

Figure 2.2: Comparison of dose depth curves for a photon beam and mono-energetic proton beam forming a Bragg peak as well as a multi-energetic proton beam forming a spread out Bragg peak [19].

2.2 Dose

To quantify the amount of radiation delivered to a target volume absorbed dose is used. The absorbed energy from radiation per unit mass [18], is given in units of Grey (Gy) where 1 Gy = 1 J/kg. Absorbed dose can be used for all types of ionizing radiation, at all energies and in all materials.

As protons transverse the human body, inelastic Coulomb scatterings and non-elastic nuclear reactions will occur. The energy from these interactions will be deposited in the tissue and the amount of energy to the amount of tissue can be quantified with absorbed dose.

The prescribed dose in a treatment plan is divided into several fractionations, irradiating a portion of the total dose in each fraction. A conventional treatment plan has a total prescribed dose of 70 Gy with 35 fractions, giving a fractionation dose of 2 Gy. This allows for repair and reoxygenation of normal tissue, leading to less severe side effects while still maintaining good tumour control [20].

To define the volume receiving the prescribed dose, three different targets are outlined, the gross tumour target volume (GTV), clinical target volume (CTV) and planning target volume (PTV). The GTV is defined by the tumour tissue that can be seen or measured [21]. A margin is applied to the GTV for suspected microscopic spread forming the CTV. Lastly a geometric margin is added to the CTV to account for organ movement and inaccuracies in delivery and position. This final volume is called the PTV.

3. Radiobiology

3.1 The radiosensitivity of tissue

The sensitivity to radiation of different tissues varies and, consequently, the effects of increased dose of radiation. When considering a treatment plan using radiation, the prescribed dose needs to be high enough to achieve tumour control yet low enough to prevent permanent damage to surrounding normal tissue. The different tissues are divided into two groups, early- and late-responding tissue.

Examples of early responding tissue is skin and oral mucosa. These tissues usually have cells with short lifespan and will therefore show effects of radiation after a few weeks. Damage to early responding tissue, if it is not too severe, tend to heal [20].

Side effects in late responding tissue usually takes months or even years to develop with examples being the spinal cord and lungs. Damage to these tissues is often due to damage to the connective tissues within, such as blood vessels, and tend to be more permanent than damage to early responding tissue. Consequently, possible irreversible damage to late responding tissue is more heavily weighted when determining a maximum radiation dose.

The response of radiation depends on several factors, among them the volume of irradiated tissue. This is called volume effects. Tissues can now be further divided into serial or parallel organisations, or a combination of both. Parallel organs have a large volume effect and is resistant to partial radiation of the organ. An example of this is the lungs. Even though a part of the long is damaged, the organ can still function. Parallel organs, even though the tissue may be sensitive, can receive higher doses in smaller volumes. Such an increase in dose can lead to improved tumour control.

Serial organs on the other hand, may lose their entire function if part of their volume is damaged. An example is the spinal cord, should a segment be severely damage it will lead to loss of function for the whole organ, in this case paralysis. The dose to a serial organ is therefore less determined by the volume and restricted by a maximum dose tolerated for even a small section. Figure 3.1 demonstrates the relationship between fraction of the

volume irradiated with a high dose and the probability of morbidity in serial versus parallel organs.

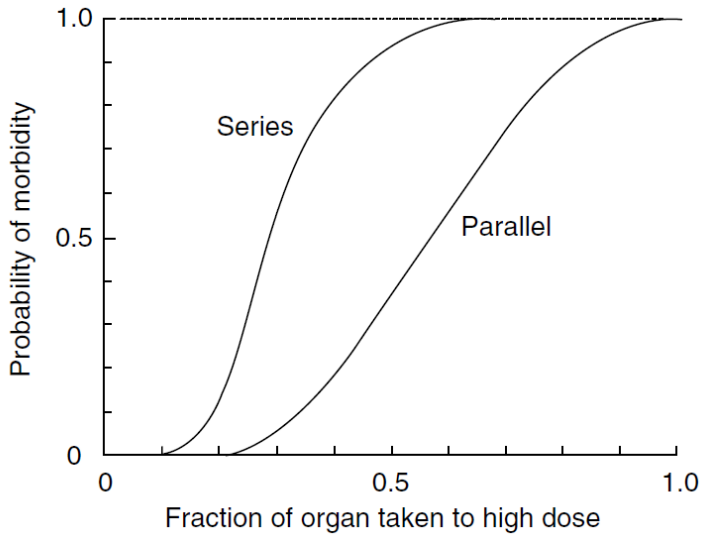

Figure 3.1: Probability of morbidity for series and parallel tissues as the fraction of the organ has received high dose [20].

To guide clinicians as to the tolerated doses and volume of each organ the Quantitative Analysis of Normal Tissue Effect in the Clinic (QUANTEC) was created. These guidelines were first published in 1991 and has since been updated as new data has come to light on three-dimensional dose, volume and outcome [22]. This summary can be used in clinics to help plan the optimal treatment plan for both tumour control and avoiding serious side effects. The QUANTEC guidelines will be compared to the different treatment plans in this thesis to ensure no limits are breached.

3.2 Quantifying biological damage of radiation

Different tissues in the human body have varying sensitivity and response to radiation. To be able to describe and predict this response the linear-quadratic (LQ) model was developed. It describes the cell survival fractions as a function of dose and is given by equation 3.1 [20].

$$S = e^{-\alpha d - \beta d^2} \tag{3.1}$$

Where d is the radiation dose for one fraction and α and β are the radiosensitive variables. α and β are not correlated and the equation can be split into an α and a β component resulting in a linear and quadratic component (eq. 3.2).

$$Linear\ or\ \alpha\ component = e^{-\alpha d} \quad (3.2a)$$

$$Quadratic\ or\ \beta\ component = e^{-\beta d^2} \quad (3.2b)$$

β represents reparable damage while α represents non-reparable damage. By fitting data to equation 3.1 cell survival curves can be made. The initial steepness off the slope is determined by the linear α. This slope is important in determining the clinical response of the tumour. Therefore, α is the dominating component when describing cell killing.

Combining the components gives the α/β ratio, with early responding tissues having a higher value and later responding tissue a lower value. In figure 3.2 the survival curves of late and early responding tissue are illustrated.

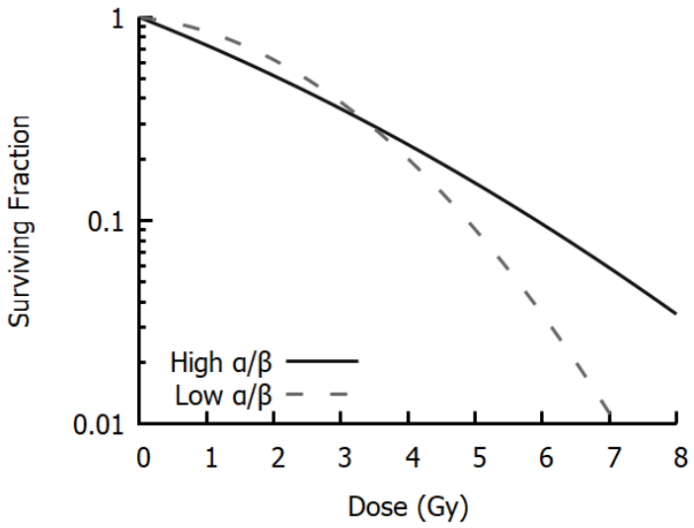

Figure 3.2: Survival curves with surviving fraction as a function of radiation dose. The dashed line is the late responding tissue with a low α/β value of 3 Gy and the solid line representing early responding tissue with a high α/β of 10 Gy [23].

Later responding tissue is more sensitive to fractionation changes than early responding tissue. The LQ model can therefore give an understanding of why fractionation works and how it can be optimised [20].

The α/β value used in head and neck patients varies from 5 to 15 Gy. For the experiments in this thesis a middle value of 10 Gy was therefore chosen.

3.3 Relative biological effectivness

Relative biological effectiveness (RBE) is defined as the dose needed to produce the same biological effect for a given radiation compared to a reference radiation (see eq. 3.3). In this thesis proton is the test radiation and photon the reference.

$$RBE = \frac{Dose\ of\ reference\ radiation}{Dose\ of\ test\ radiation} \tag{3.3}$$

For practical reasons a constant RBE of 1.1 is often used clinically, however RBE depend on multiple factors such as dose fractionation, irradiated tissue and LET [2]. RBE can therefore vary by implementing the LQ model (eq. 3.4) [24].

$$RBE\left[D_p, \alpha, \alpha_x, \beta, \beta_x\right] = \frac{1}{2D_p}\left(\sqrt{\left(\frac{\alpha_x}{\beta_x}\right)^2 + 4D_p\frac{\alpha_x}{\beta_x}\frac{\alpha}{\alpha_x} + 4D_p^2\frac{\beta}{\beta_x}} - \frac{\alpha_x}{\beta_x}\right) \tag{3.4}$$

Where D_p is the physical dose, α and β are radiosensitive parameters for protons, α_x and β_x radiosensitive parameters for photons as the reference radiation. Looking at the limits where the physical dose goes towards zero and infinity, RBE_{max} and RBE_{min} can be defined. Now RBE_{max} only depends on the α values and RBE_{min} on the β (see eq. 3.5-3.6).

$$\lim_{D_p \to 0} RBE = RBE_{max} = \frac{\alpha}{\alpha_x} \tag{3.5}$$

$$\lim_{D_p \to \infty} RBE = RBE_{min} = \sqrt{\beta/\beta_x} \tag{3.6}$$

Combining equation 3.4-3.6 results in the following equation (eq. 3.7);

$$RBE\left[D_p, (\alpha/\beta)_x, RBE_{max}, RBE_{min}\right] = \frac{1}{2D_p}\left(\sqrt{\left(\frac{\alpha}{\beta}\right)_x^2 + 4D_p\left(\frac{\alpha}{\beta}\right)_x RBE_{max} + 4D_p^2 RBE_{min}^2} - \left(\frac{\alpha}{\beta}\right)_x\right) \tag{3.7}$$

Where $(\alpha/\beta)_x$ is the α/β ratio for photons, the reference radiation. Now the proton specific variables are contained in RBE_{max} and RBE_{min}. Different RBE models tries to find the optimal expressions for these variables, as well as potentially expanding the expression.

4. Hypoxia

4.1 Definition

Tumours with a very low amount of oxygen is called hypoxic, whereas a well oxygenated tumour is called normoxic. Hypoxia is usually defined as cells with pO_2 lower than 8-10 mmHg [6] while normoxic cells have pO_2 up to 100 mmHg (see table 4.1 for normoxic values in different tissues). pO_2 is the oxygen partial pressure and reflects the relationship between oxygen consumption and delivery [7].

Table 4.1: Normoxic mean values expressed in percentage (=1.013 kPa) and mmHg (=133.322 Pa) for different human tissues [7].

	pO_2	
	mmHg	%
Air	160	21.1
Inspired air (in the tracheus)	150	19.7
Air in the alveoli	110	14.5
Arterial blood	100	13.2
Venous blood	40	5.3
Cell	9.9-19	1.3-2.5
Mitochondria	<9.9	<1.3
Brain	33.8 ± 2.6	4.4 ± 0.3
Lung	42.8	5.6
Skin (sub-papillary plexus)	35.2 ± 8	4.6 ± 1.1
Skin (dermal papillae)	24 ± 6.4	3.2 ± 0.8
Skin (superficial region)	8 ± 3.2	1.1 ± 0.4
Intestinal tissue	57.6 ± 2.3	7.6 ± 0.3
Liver	40.6 ± 5.4	5.4 ± 0.7
Kidney	72 ± 20	9.5 ± 2.6
Muscle	29.2 ± 1.8	3.8 ± 0.2
Bone marrow	48.9 ± 4.5	6.4 ± 0.6

Hypoxic tumours arise as tumour cells proliferate at an increasing speed, leading to increased metabolic demand. Moreover, tumours can have disorganised vascular architecture leading to less efficient delivery of oxygen. There is then an imbalance between oxygen supply and consumption [25].

One divides hypoxia into two different categories; chronic and acute. Chronic hypoxia, also called diffusion-limited hypoxia, is caused by disorganised vascular architecture in the tumour. This entails that the distance between microvessels is larger than normal due to the increased proliferation speed of tumours. Consequently, the diffusion distance from the nearest capillary is increased compared to healthy tissue. If the distance between a blood vessel and a cell is higher than 150 μm, oxygen will not be able to diffuse into the cell [26], as is illustrated in figure 4.1. Furthermore, can prolonged blood oxygen reduction due to anaemia and adverse vascular geometry cause chronic hypoxia.

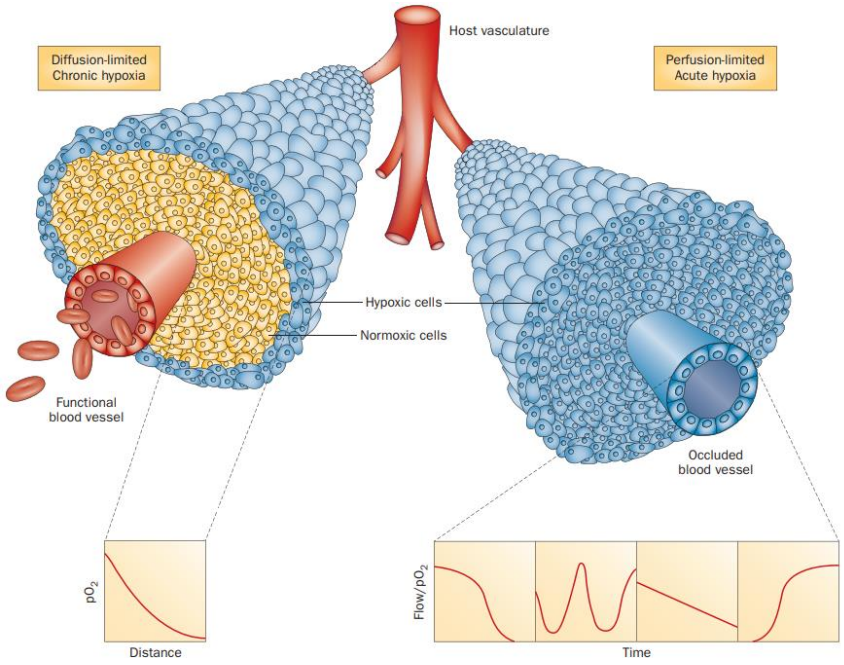

Figure 4.1: Illustrates diffusion-limited chronic hypoxia on the left and perfusion-limited acute hypoxia on the right. pO_2 as a function of distance is shown for chronic hypoxia, illustrating the gradual decrease in oxygen moving away from the blood vessel. For acute hypoxia flow/pO_2 is shown as a function of time illustrating the initial shutdown, repeated fluctuations, a gradual decrease and lastly the recovery [27].

Acute also called perfusion-limited hypoxia, is caused by temporarily reduced perfusion leading to fluctuations in tumour blood flow [25]. In figure 4.1 this can be seen in the flow/pO_2 as a function of time plot, where from left to right is meant to illustrate the initial shutdown of blood flow and oxygen, repeated fluctuations, a gradual decrease and lastly the recovery. Examples of factors leading to the initial shutdown are circulating tumour cells or blood plugging vessels and vessel collapse due to high interstitial pressure [27].

4.2 Oxygen enhancement ratio

The amount of oxygen within a cell affects the biological effect of radiation. This is called the oxygen effect. Ionisation damage can be afflicted in two ways, indirect and direct action. Direct action directly ionizes the DNA within the target cell, whereas indirect action produces free radicals. These free radicals can then damage the DNA as free radicals form, in the presence of oxygen, peroxides which is toxic to DNA and cause irreparable damage [26]. Since indirect action dominate at low LET, the amount of damage done during low-LET radiotherapy such as with photons, can be significantly reduced by low oxygen pressure. For radiation with higher LET the oxygen effect will be less pronounced as seen in figure 4.2B and will vary depending on the LET.

The oxygen enhancement ratio (OER) is defined as the ratio of dose needed to produce the same amount of biological damage in hypoxic (D_h) and normoxic (D_n) tissue. It is a way of quantifying the increased radioresistance of hypoxic cells [28], see equation 4.1.

$$OER = \frac{D_h}{D_n} \tag{4.1}$$

Figure 4.2 shows graphically OER dependency on LET and pO_2, where in A) we see the OER dependence on pO_2, in B) OER dependence on LET and in panel C) we see OER dependence on both pO_2 and LET. We can see that the OER decreases as the LET, the pO_2 or both increase.

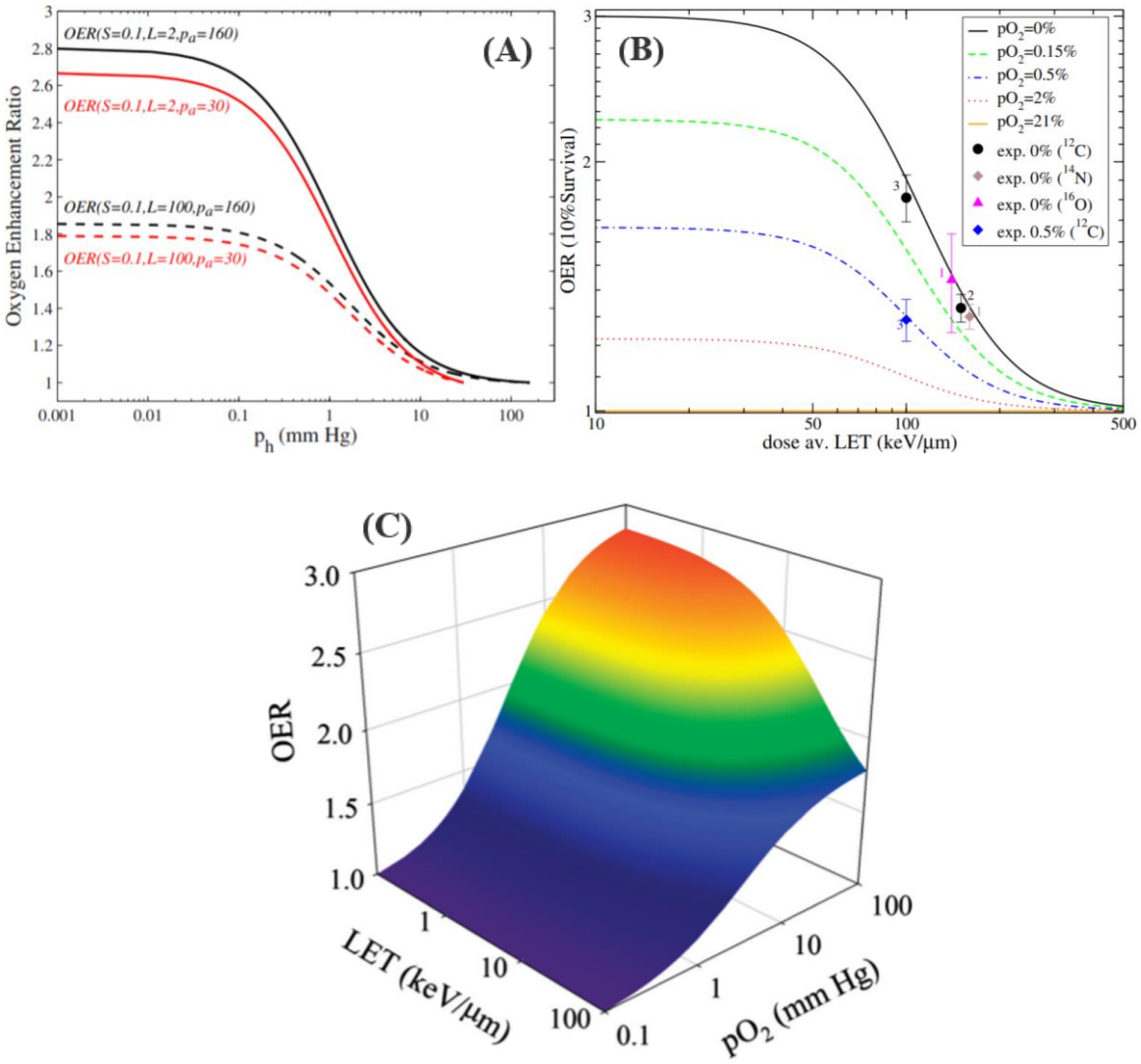

Figure 4.2: (A) OER dependent on hypoxic partial pressure ph for normoxic pO_2 at 160 mmHg and 30 mmHg at 10 % survival. Solid lines are at low LET and dashed lines at high LET [28]. (B) OER dependent on LET at different pO_2 values [29]. (C) OER as a function of LET and pO_2 (Malinen and Sovik, 2015).

The OER is similar for protons and photons at low LET, but as the LET for protons increase with decreasing energy, the OER decreases. This effect is even more pronounced for heavier ions with high LET such as carbon ions. By implementing the LQ model, OER can also be expressed as in equation 4.2 [28].

$$OER(S, L, p_a, p_h) = \frac{\sqrt{\alpha^2(L,\ p_h) - 4\beta(L, p_h) \cdot ln\, S} - \alpha(L, p_h)}{\sqrt{\alpha^2(L,\ p_a) - 4\beta(L, p_a) \cdot ln\, S} - \alpha(L, p_a)} \cdot \frac{\beta(L, p_a)}{\beta(L, p_h)} \qquad (4.2)$$

Where S is the survival fraction, L is the LET, p_h is pO_2 under hypoxic conditions, p_a is pO_2 under aerobic conditions ($p_h \leq p_a$), α expressed in equation 4.3 and β expressed in equation 4.4.

$$\alpha(L,p) = \frac{(a_1 + a_2 \cdot L) \cdot p + (a_3 + a_4 \cdot L) \cdot K}{p + K} \tag{4.3}$$

$$\sqrt{\beta(L,p)} = \sqrt{\beta(p)} = \frac{b_1 \cdot p + b_2 \cdot K}{p + K} \tag{4.4}$$

Where p is the pO_2, L is the LET, a_1, a_2, a_3, a_4, b_1 and b_2 are constants obtained by fitting in vitro experimental data and K is the oxygen level at which the relative radiosensitivity (biological response to radiation as a function of p) is equal to the mean of the maximum radiosensitivity and 1. K is often set to be 3 mmHg.

Thus, the OER depends on both the LET and pO_2 [6].

If one can define the hypoxic regions in the tumour, treatment can be individualised and adapted to better treat the patient. Different methods are being studied, for instance dose painting. Here, using for example PET (positron emission tomography) images to define the hypoxic regions, one can increase the dose accordingly with intensity-modulated radiation therapy (IMRT) [3]. More on dose painting and other methods in chapter 4.4.

4.3 Imaging hypoxia with PET

To take hypoxia into consideration in radiotherapy, one must first be able to image it. Ideally the imaging method should be non-invasive, readily available, repeatable and accurate. The most widespread method nowadays for detecting hypoxia is PET. Several different tracers are used, with ^{18}F labelled nitroimidazole based tracers being the most common [27]. The patient studied in this thesis had PET images taken with both 2-(2-nitro-1H-imidazol-1-yl)-N-(2,2,3,3,3-pentafluoropropyl)-acetamide ([^{18}F]EF5). and fluorodeoxyglucose ([^{18}F]FDG) as tracers.

When imaging with PET the patient must first be injected with a radioactive isotope, a tracer. As the tracer hopefully reaches the tumour, it will decay by positron emission. After a short distance the positron will annihilate with an electron, producing two 511 keV photons. These photons will then travel in the opposite directions [30]. Placed around the patient is a ring of detectors recording the emitted photons. From this a line of response can be found, as illustrated in figure 4.3. Conventionally by recording many line of responses, overlapping lines show the areas with the highest signals.

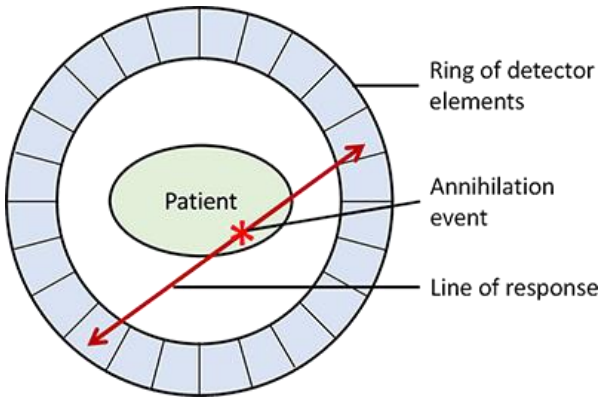

Figure 4.3: Illustrates the basic function of a PET detector. After the annihilation occurs, the photons are emitted in opposite directions before they are detected by the ring of detectors [31].

PET has a great potential for detecting hypoxia. It is non-invasive, can be used to detect tumours in the whole body and has the possibility of developing tracers for specific needs [26]. There are several different characteristics that are important in a tracer. However, the most important characteristics for hypoxia detection is a correlation between uptake and the pO_2 levels of the cells. The tracer should be able to enter all types of cells and only be able to leave in the presence of oxygen [25].

The first tracer used for PET image acquisition for the patient studied in this thesis is [^{18}F]EF5. It is a nitroimidazole compound labelled with fluorine tracer. Nitroimidazole tracers can diffuse through the cell membrane where they reduce into reactive metabolites by intracellular reductases. This process is dependent on the level of oxygen in the tumour. Under hypoxic conditions further reductions will occur, irreversibly trapping the tracer in the cell. However, under normoxic conditions the tracer will be re-oxidised and diffuse out of the cell [25].

[^{18}F]EF5 as a tracer it is very stable and has an even biodistribution. Furthermore, the metabolism of [^{18}F]EF5 in humans is negligible. This allows for higher specificity of hypoxia related binding of the tracer, as well as improved image quality. A disadvantage however is the complicated radiochemical synthesis which limits a larger utilization of the tracer if the process is not simplified. Another possible disadvantage is the increased lipophilicity compared to other nitroimidazole tracers. This will make it easier to enter cell membranes and give a uniform distribution in the whole body, but also enter the background tissues and have a slower elimination rate. This can lead to a decreased target-to-background contrast.

The other tracer used is [^{18}F]FDG. Unlike [^{18}F]EF5, [^{18}F]FDG is not a nitroimidazole compound, but glucose based and is the most commonly used PET tracer. One can exploit the highly enhanced glycolysis in cancer cells, called the Warburg effect [26], to use [^{18}F]FDG as a tracer. Furthermore, it can detect hypoxia as under hypoxic conditions there are increased levels of glucose transporter proteins GLUT-1 and GLUT-3, and a correlation between them and [^{18}F]FDG uptake [32]. Unlike glucose, [^{18}F]FDG stops after the first step of glycolysis and ends up trapped in the cell, giving good target-to-background contrast. The target-to-background contrast is further improved by the ability for [^{18}F]FDG to be excreted in urine leading to rapid blood clearance. However, several conditions can affect the specificity of the images. False positive uptake can be triggered by infections, inflammation and so on, leading to misidentified malignancies. Furthermore, the images may be affected by the metabolic activity in the background tissue.

4.4 Hypoxia treatment adaptations

Do to the increased radioresistance of hypoxic cells, alternative treatment is needed to provide equal amount of cell killing compared to normoxic tumours.
An analysis of hypoxia imaging information for use for treatment adaptations can be done with both qualitative and quantitative methods. A qualitative analysis can for example be painting by contours. This is done by defining larger subvolumes of hypoxia from the imaging information by setting different threshold values for what is defined as hypoxic and normoxic. A higher dose is then prescribed to the hypoxic subvolumes than the remaining

tumour to counteract hypoxia. A quantitative evaluation, however, trust the image information more and uses the signal values to determine specific pO_2 levels, and adjusting treatment thereafter [33]. An example is voxel-by-voxel dose painting, where the tumour is divided into voxels and each voxel are assigned a pO_2 value. The dose can then be adjusted for each individual voxel.

4.4.1 Dose painting

Toma-Dasu et al. [34] demonstrates the importance of including different uptake conversion functions for different tracers. They compare the uptake of the PET tracers [^{18}F]FMISO and [^{18}F]FETA, were [^{18}F]FETA has a lower uptake for intermediate oxygen tensions than [^{18}F]FMISO [34].

The same conversion function is used for both tracers and the CTV, GTV and hypoxic core are prescribed doses according to the calculated uptake. This leads to a significantly lower prescribed dose to the hypoxic core for [^{18}F]FETA compared to [^{18}F]FMISO (see table 4.2). Furthermore, the authors look at what would happen if one where to assume a linear dependency of the intensities for the dose modifying factor. This was done by setting the dose modifying factor (eq. 4.6) for the minimum tracer uptake to 1 and the maximum to 3 (fully hypoxic conditions). This demonstrated the importance of not using a linear approximation as in this example the dose to the hypoxic core is significantly higher, potentially irradiating healthy tissue with unnecessarily high dose levels.

Table 4.2: Prescribed dose to CTV, GTV and hypoxic core for [^{18}F]FMISO, [^{18}F]FETA and linear approximation using the same image intensities and uptake functions [34].

Conversion curve	**Mean dose (Gy)**		
	CTV	**GTV**	**Hypoxic core**
[^{18}F]FMISO	59	66	85
[^{18}F]FETA	56	60	62
Linear approximation	57	63	105

To achieve the proper algorithm for the individual tracers, experimental data is first fitted to parameters in an uptake equation. In Toma-Dasu et al. [9] they used equation 4.5 and data form seven patients with [^{18}F]FMISO PET/CT (computed tomography) images taken at the start of therapy. The uptake per voxel is given by the three fitted variables, *A*, *B* and *C*, and pO_2 which is the oxygen partial pressure.

$$Uptake = A - \frac{B \times pO_2}{C + pO_2} \tag{4.5}$$

When the uptake based on the PET image signals is found, the dose modification due to the increased radioresistance needs to be calculated. This can be done by using equation 4.6 [9] where *f* is the dose modification factor for photons, pO_2 the oxygen partial pressure, *k* is the same as *K* in equation 4.3 and 4.4, and OER_{max} is the maximum OER achieved in the absence of oxygen.

$$f = \frac{OER_{max}(k + pO_2)}{k + OER_{max} \times pO_2} \tag{4.6}$$

The relationship between pO_2, uptake of [^{18}F]FMISO and f is illustrated in figure 4.4.

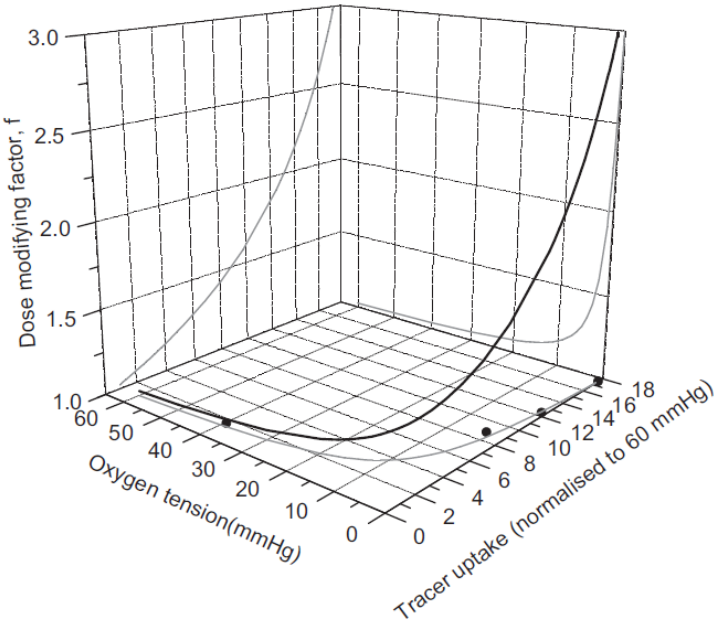

Figure 4.4: Shows the relationship between oxygen tension, [^{18}F]FMISO tracer uptake and the resulting dose modifying factor [9].

From the dose modification factor a heterogeneous dose prescription can be made. For patients with non-hypoxic tumours, the resulting dose in this study is close to the dose in routine practice today. For patients with hypoxic tumours however, there could be a large improvement from individualized treatment. In the study a patient with a hypoxic tumour (the pO_2 threshold for hypoxic region set at 10 mmHg) had a calculated dose of 66 Gy to GTV, 73 Gy to CTV and 98 Gy to HTV (hypoxic target volume) for a segmented dose distribution using IMRT [9]. Whereas a homogenous dose delivery was calculated to 77 Gy. Figure 4.5 shows tracer uptake, dose modification factor and dose distribution for this patient.

The hypoxic region is centred in the tumour, leading to an increased dose to this region and a lower dose requirement (11 Gy less then homogenous dose) for the periphery. This could spare the normal surrounding tissue and lead to improved local control, compared to the homogenous dose. By incorporating hypoxia information in treatment planning, patients which were previously unresponsive to treatment could have an increased chance of local control.

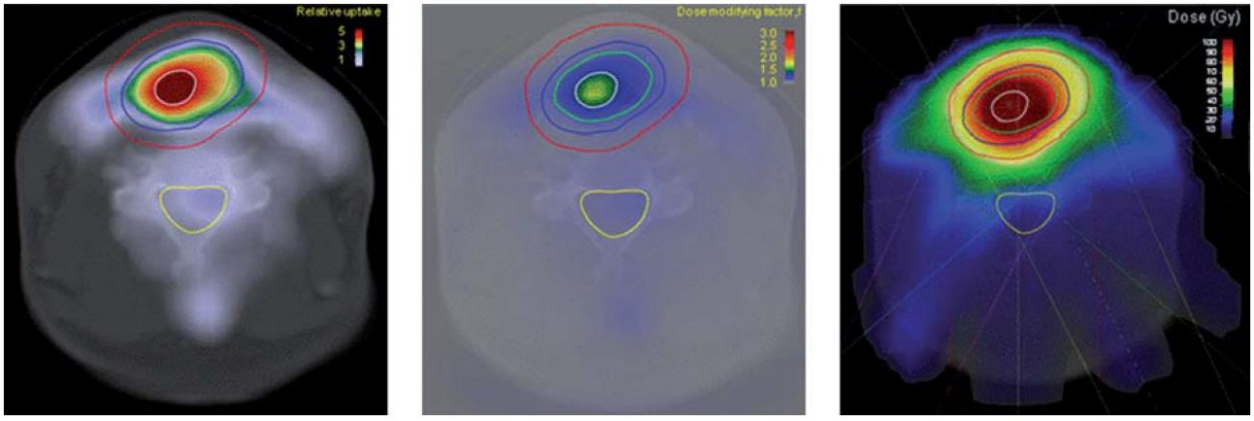

Figure 4.5: The picture to the left shows the [^{18}F]FMISO uptake, in the middle the calculated dose modifying factor and to the right the resulting dose distribution. The GTV, CTV and PTV are contoured with green, blue and red respectively as well as the hypoxic region in white. The pictures are made using ORBIT workstation and data from patient 1 in "Dose prescription and treatment planning based on FMISO-PET hypoxia" [9].

Dose painting with photons can be challenging due to the steep dose gradients needed between hypoxic and normoxic regions in the tumour. Therapeutic photon beams have physical limitations to the steepness that can be achieved. With ions on the other hand, the total energy is deposited over a narrow Bragg peak, making it possible to achieve steeper gradients and better dose conformation. Malinen and Sovik [3] studied prescribing ion

beams on a voxel-by-voxel basis using dynamic-contrast-enhanced magnetic resonance imaging (DCE-MRI) to map the spatial distribution and extent of hypoxic regions.

MRI is a non-invasive, non-ionising imaging modality. By utilizing the spin of hydrogen nuclei, a signal is produced by placing the patient inside a strong magnet with additional magnetic gradients and radio frequency coils [35]. DCE-MRI measures perfusion as well as tissue permeability [26] by using gadolinium, a paramagnetic contrast agent. The method indirectly measure hypoxia by looking at blood flow and blood volume in tissue. Hypoxia can then possibly be detected through inadequate blood flow.

Tumour control probability (TCP) is defined as the probability for a tumour to be eradicated or controlled at a given prescribed dose [36]. The optimal dose distribution per voxel i and treatment fraction j yielding maximum TCP was calculated by using equation 4.7:

$$\frac{\alpha_{ij}}{(\alpha_{ij}/\beta_{ij})} {d_{ij}}^2 + \left(\alpha_{ij} - \frac{2}{(\alpha_{ij}/\beta_{ij})}\right) d_{ij} - d_r \left[\alpha_r \left(1 + \frac{d_r}{(\alpha_r/\beta_r)}\right) - \frac{2}{(\alpha_r/\beta_r)}\right] - ln\left(\frac{p_i \alpha_{ij}}{p_r \alpha_r}\right) = 0 \quad (4.7)$$

where α and β are the linear and quadratic components of radiosensitivity, p the cell density, d dose, i voxel, j fraction, r reference value which for p is the initial cell density, d the mean tumour dose, and for α and β are set to the mean parameter dose taken over the tumour.

The calculated dose distribution can then be used for dose painting during treatment. Dose painting, LET painting and pO_2 map for the first treatment fraction are shown in figure 4.6. We can see that voxels with low pO_2 levels are prescribed increased values of dose and LET.

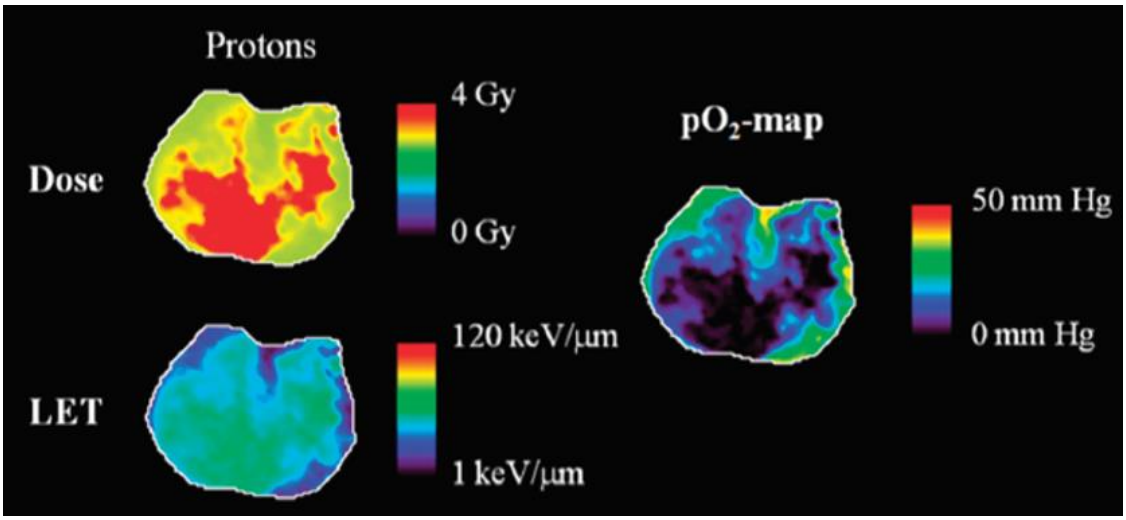

Figure 4.6: Maps showing optimal dose and LET distribution, as well as pO_2 map for a single slice of the tumour before the first treatment fraction [3].

4.4.2 LET painting

LET painting can potentially be used to counter hypoxic tumours. As previously mentioned, LET and OER are connected, therefore as LET increase the OER decreases. The proton beam is given as a SOBP, a plateau of different LETs combined. By targeting the most hypoxic regions with the highest LET those regions will have lower OER compared to conventional photon therapy and thus easier to kill. The highest Bragg peaks are then given to hypoxic regions on a voxel-by-voxel basis, while the plateau of lower LET is targeted on the normoxic regions. This will lead to a homogenous SOBP LET spectrum heterogeneously redistributed, while keeping the tumour dose constant.

Malinen and Sovik [3] compare the TCP and therapeutic gain of dose painting, LET painting and combined LET/dose painting using protons. Therapeutic gain is defined as the difference between conventional therapy and hypoxia painting mean tumour doses giving an iso-effect of 50% TCP. The result is illustrated in table 4.3 and figure 4.7.

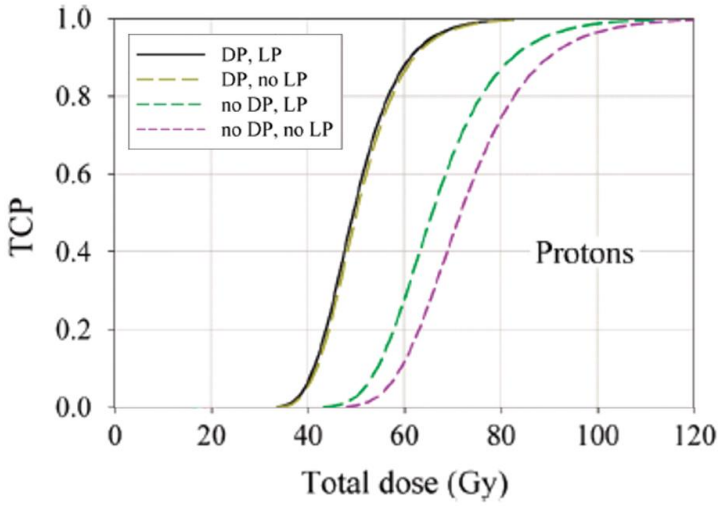

Figure 4.7: The graph shows the tumour control probability (TCP) as a function of tumour dose for protons using four different strategies. These are combined dose and LET painting (DP, LP), dose painting (DP, no LP), LET painting (no DP, LP) and conventional radiotherapy (no DP, no LP) [3].

All methods studied gave improved TCP and therapeutic gain compared to conventional therapy. LET painting improved therapeutic gain by 9% whereas dose painting showed an 43% improvement. Highest of them all are combined LET/dose painting, however it is only 2% more than dose painting alone. Thus, it could indicate that dose painting is more important to implement than LET painting for protons.

Table 4.3: Therapeutic gain from no painting (conventional therapy), LET painting, dose painting and combined dose and LET painting for protons [3].

Ion species	**No painting**	**LET**	**Dose**	**Combined**
Protons	1.00	1.09	1.43	1.45

Moreover, the impact of number of treatment fractions with replanning were studied for combined LET/Dose painting. Replanning is done by acquiring new images to obtain an updated pO_2 distribution and replan the LET/Dose painting thereafter.

Table 4.4 shows this given in therapeutic gain, which increases with the number of replans. However, the largest improvement per planning session is after just one extra replanning, indicating large increase in therapeutic gain can be achieved without replanning needed after each session.

Table 4.4: Therapeutic gain from replanning using combined dose and LET painting. Conventional treatment with no painting and homogenous tumour dose is shown as zero planning sessions [3].

Combined dose and LET painting					
Number of planning sessions	0	1	2	4	16
Therapeutic gain	1.00	1.24	1.38	1.43	1.45

The authors assumed however that the beam can be perfectly distributed voxel-by-voxel, that TCP reflect dose prescription perfectly reproduced in the tumour and does not take into consideration complication probabilities for normal tissue and organs at risk. As such the estimates must be seen as an upper limit for what is possible therapeutic gains.

4.4.3 RBE and OER weighted dose

For the methods mentioned previously, OER has been used for the calculations. With RBE and OER weighted dose (ROWD) in addition to OER, RBE is also considered. RBE is the ratio of dose needed to produce the same biological damage of photons compared to a given radiation, in this case protons [2]. The RBE of protons is often set to 1.1 for practical reasons, however RBE varies with, among other things, LET and is therefore not constant. Several alternative models exist, one of them being the Rørvik RBE model [5].

In Dahle et al. [6] a ROWD was calculated using a FLUKA Monte Carlo based tool and then optimized taking into consideration PTV and OARs (organs at risk). The OER used was based on equation 4.2 with surviving fraction, S=0.1, while for the RBE both constant RBE of 1.1 and the Rørvik RBE model [5] were used separately to compared them. Equation 4.8, 4.9 and 4.10 were used to calculate the ROWD on a voxel-by-voxel basis for proton therapy [6].

$$D_{OER,RBE} = \frac{D}{D_p}\left(\sqrt{\left(\frac{\alpha_x}{2\beta_x}\right)^2 + \frac{\alpha_h D_p + \beta_h D_p^2}{\beta_x}} - \frac{\alpha_x}{2\beta_x}\right) \tag{4.8}$$

$$\alpha_h = \frac{\alpha_a}{OER(L, p_h)} \tag{4.9}$$

$$\beta_h = \frac{\beta_a}{OER^2(L, p_h)} \quad (4.10)$$

Where α_x and β_x are the aerobic photon radiosensitivity parameters, α_a and β_a are the aerobic proton radiosensitivity parameters, whereas α_h and β_h are hypoxic proton radiosensitivity parameters. OER is as mentioned based on equation 4.2 with S=0.1, D the total physical dose and D_p proton physical dose. The different dose distributions will be referred to as $D_{OER,RBE1.1}$ (OER and RBE1.1), $D_{OER,ROR}$ (OER and Rørvik RBE model) and $D_{RBE1.1}$ (OER=1 i.e., not accounting for hypoxia).

The estimated ROWD distributions were studied both in a water phantom and a HNC patient, where the water phantom was divided into seven parts with different pO_2 values from 2.5 to 30 mmHg, while the pO_2 levels for the patient were obtained from [^{18}F]EF5 PET images. Moreover, dose distributions from using single and opposing beams were compared.

In the water phantom the ROWD (see figure 4.8) where optimized to the prescribed median target dose of 2 Gy(RBE). To be able to counteract the hypoxic tissue and radiate the prescribed dose, a higher physical dose is needed. For the most hypoxic region of the water phantom the OER is approximately 1.45. A sufficient increase in biological dose was not obtained when only using one field for $D_{OER,RBE1.1}$ and $D_{OER,ROR}$. By using opposing beams however, the necessary biological dose could be achieved although less homogenously than for $D_{RBE1.1}$. Furthermore, the ROWD is more heterogeneous close to the borders of the different pO_2 levels. This, however, would be impossible to counteract without having perfectly rectangular physical dose distributions.

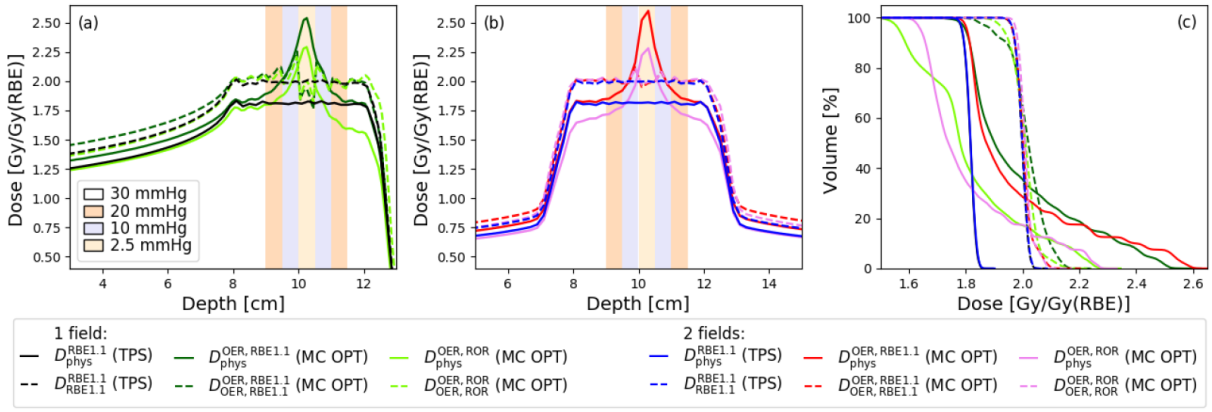

Figure 4.8: Shows the spread-out Bragg peak in the water phantom for a) single field and b) opposing fields, while c) is the corresponding dose volume histograms. $D_{RBE1.1}$, $D_{OER,RBE1.1}$ and $D_{OER,ROR}$ distributions for physical (solid lines) and biological dose (dashed lines) [6].

For the HNC patient only RBE of 1.1 was used. The patient was prescribed a dose of 70 Gy over 35 treatment fractions. The optimized treatment plans using ROWD with RBE of 1.1 achieve a median PTV dose of 70.8 Gy(RBE), in good agreement of the prescribed dose. However, the $D_{OER,RBE1.1}$ plan has the lowest biological dose at the hypoxic regions, as seen in figure 4.9. This indicate that the plan was not able to deliver high enough physical dose without violating tissue constraints. The dose to OAR (left parotid gland) was also increased.

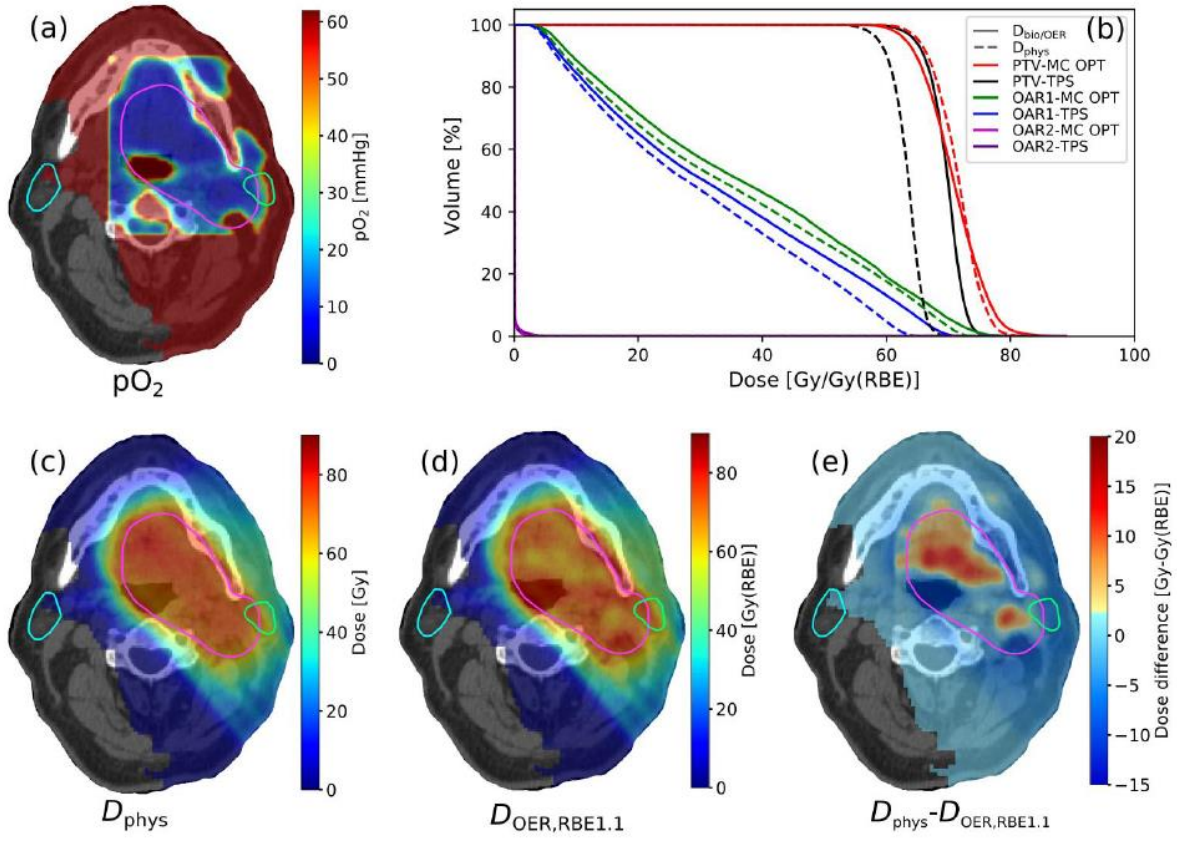

Figure 4.9: The HNC patient a) pO_2 map, b) dose volume histograms, c) physical dose, d) $D_{OER,RBE1.1}$ and e) the dose difference between physical dose and $D_{OER,RBE1.1}$. The pink delineation is the PTV, green the left parotid gland and cyan the right parotid gland, the glands are OARs[6].

From the results of the water phantom and HNC patient one can see that the method manages to have an increased physical dose to hypoxic regions, leading to a biological dose close to the prescribed dose.

5. Methods

The aim was to define different pO_2 thresholds to determine the hypoxic volumes using Eclipse treatment planning system and [^{18}F]EF5 PET/CT images. Then calculate the OER and RBE weighted dose received through FLUKA Monte Carlo simulations using the OER model by Dahle et al. [6], constant RBE of 1.1 and the Rørvik weighted RBE model [5]. Afterwards the physical dose needs to be adjusted with an OER factor for each different pO_2 threshold before studying the biological dose received.

5.1 Patient data and treatment planning

The patient images studied in this thesis were acquired at Turku University Hospital. The initial acquisition and clinical studies were approved by the Ethics Committee of Hospital District of Southwest Finland [37]. The patient has untreated pharyngeal squamous cell carcinoma on the base of the tongue. Three sets of PET/CT pictures were acquired, two with [^{18}F]EF5 using the same GE D690 PET/CT scanner and one with [^{18}F]FDG with a Discovery VCT PET/CT scanner, with CT pictures taken right before acquisition. Furthermore, a flat scanner table with thermoplastic mask was used for immobilization.

Varian's Eclipse treatment planning system version 15.1 was used to make the treatment plans for the patient. Eclipse is used by thousands of treatment centres all over the world and allows for dose calculations and optimization which can then be used by the radiotherapy delivery machine for treatment [38].

The most common means of proton therapy delivery is intensity modulated proton therapy (IMPT) [39]. The fluence of each beam is adjusted to be nonuniform, allowing for increased dose conformity [2]. This is done in Eclipse with spots. Each field is made of several spots with different weights as seen in figure 5.1. The field is furthermore divided into different energy layers as it transverse the patient, where for each layer the spots will have different weights.

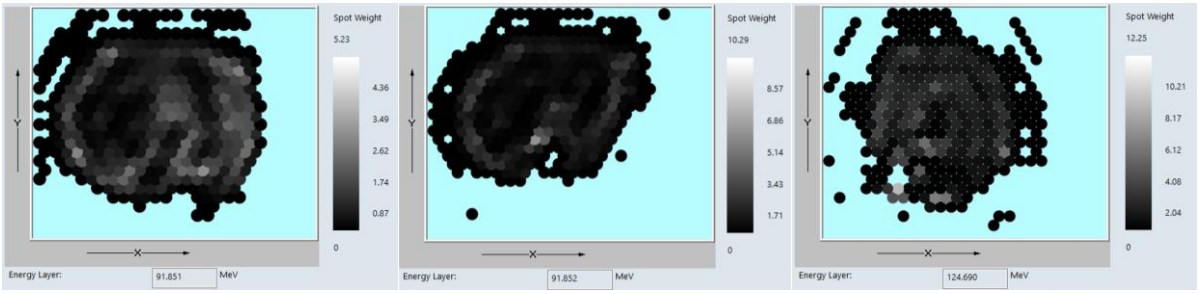

Field 1 **Field 2** **Field 3**

Figure 5.1: Shows the spot distribution and weight for the middle energy layer of each field in the original treatment plan. At the left is layer 9/17 for field 1, in the middle layer 8/16 for field 2 and to the right layer 12/24 for field 3.

To start the process, CT and PET pictures were imported into Eclipse. Using the image registration tab, the CT and the first set of PET [^{18}F]EF5, images were matched with auto registration followed by visual verification. This was done by looking at the anatomy of the bones and making sure they overlapped in the PET and CT images. To correlate the [^{18}F]EF5 uptake in Bq/ml with the pO_2 values, equation 5.1 was used. The parameters A = 2.60, B = 1.98 and C = 2.50 mmHg are reaction-specific parameters from Dahle et al. [6] and the different thresholds were inserted as pO_2 values. The resulting uptake is given in SUV (standard uptake value), which is the activity in the region of interest per unit volume divided by the injected activity per whole body mass [26]. The result from equation 5.1 was therefore multiplied with a normalization factor of 1298.1 Bq/ml.

$$Uptake\ [SUV] = A - \frac{B \cdot pO_2}{C + pO_2} \tag{5.1}$$

The resulting uptake in Bq/ml for the different pO_2 threshold values is given in table 5.1.

Table 5.1: The results using equation 5.1 in SUV and Bq/ml for threshold values 10 mmHg, 7.5 mmHg and 5 mmHg.

pO_2	Uptake [SUV]	Uptake [Bq/ml]
10 mmHg	1.02	1319
7.5 mmHg	1.12	1447
5 mmHg	1.28	1662

The widow level in Eclipse was used to adjust the Bq/ml value visible in the PET images. The different pO_2 threshold Bq/ml values were adjusted, and the resulting regions segmented forming the hypoxic structures as can be seen in figure 5.2. In table 5.2 the minimum, maximum and mean values of the uptake are shown, as well as the volume of the hypoxic regions and the PTV.

For all the three hypoxic subvolumes, the minimum uptake Bq/ml is lower than that of the estimated threshold in table 5.1. This difference is likely due to small points or volumes within the structure with higher pO_2 values that were too small to either see or be excluded from the volume. Furthermore, some of the pO_2 thresholds led to quite complex shapes and the contouring tool cannot always conform perfectly to these complex shapes. Small parts of the tumour with higher pO_2 than the thresholds may therefore have been included in the hypoxic volume, resulting in lower uptake than expected.

Figure 5.2: The different hypoxic volume view from the right side of the patient with threshold values 10 mmHg (yellow), 7.5 mmHg (red) and 5 mmHg (blue).

Table 5.2: The minimum, maximum and mean of the uptake and volume for the threshold values 10 mmHg, 7.5 mmHg and 5 mmHg as well as the PTV.

Volume	**Min [Bq/ml]**	**Max [Bq/ml]**	**Mean [Bq/ml]**	**Volume [cm^3]**
10 mmHg	1231.9	2173.1	1529.9	67.6
7.5 mmHg	1396.7	2173.1	1618.1	40.3
5 mmHg	1634.6	2173.1	1798.0	10.4
PTV	528.2	2173.1	1297.7	139.8

With the new structures in place, the treatment plan can be optimized. Three fields were placed on the left side of the patient with a total dose of 70 Gy over 35 fractions as can be seen in figure 5.3.

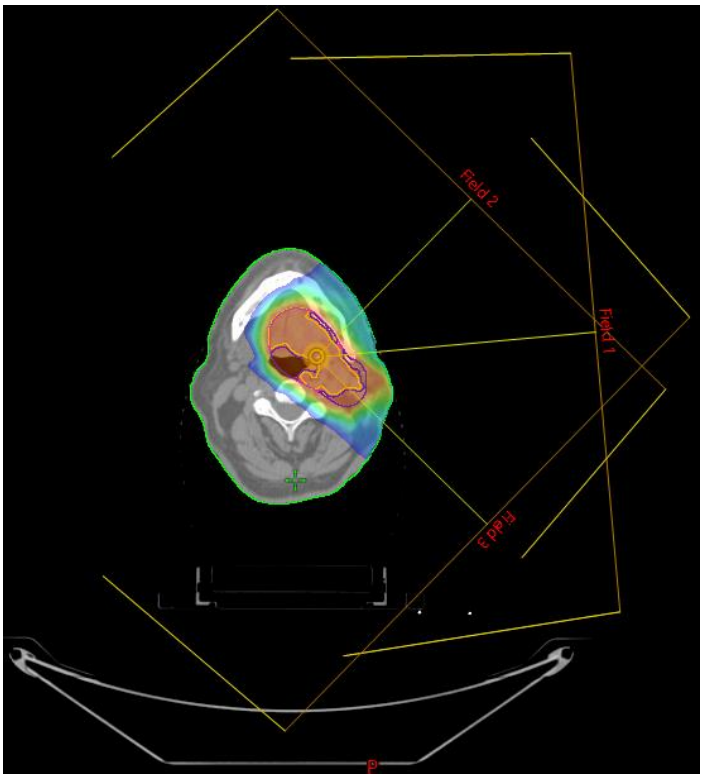

Figure 5.3: Treatment field setup in Eclipse viewed from underneath, mirroring the image. Three fields were placed on the lefthand side of the patient, here shown on the right side of the figure.

Dose objectives were set to an upper and lower limit of 71.5 Gy and 68.5 Gy for the PTV and an upper limit of the prescribed dose to the left parotid gland, as it overlaps with the PTV. No other OARs were taken into consideration for the optimisation.

For the optimization the multifield optimization algorithm CAPNUPO was used as well as CAPPCS as the calculation algorithm. Lastly, the CT images, plan, structure set and dose plan were exported as DICOM files to be recalculated in FLUKA.

5.2 Monte Carlo simulation

Eclipse calculates the expected dose distribution for the treatment plan, however it does not include OER in its calculations. Furthermore, no RBE models other than a constant RBE of

1.1 can be chosen, neither can a LET distribution be studied. To be able to include the OER and different RBE models as well as further analysis of the doses, the treatment plan needs to be recalculated.

For the recalculation, FLUKA with FLAIR (FLUKA Advanced Interface) was used. FLUKA is a Monte Carlo simulation tool developed by CERN and the Italian National Institute for Nuclear Physics. With a range of about 60 different particles one can simulate the particles propagation and interactions in matter.

FLUKA can be quite difficult to use and is prone to syntax errors. FLAIR was therefore developed as an application programming interface for FLUKA [40]. There are no command line interactions needed, one can easily edit input files and check for errors, and it also provides post processing of the output. It has a database with all known nuclides for incoming particles and about 300 different materials for possible targets.

The Monte Carlo method is a collection of different techniques used to solve complex problems, that all implement the use of random samples. It is widely used to simulate physical and biological systems. When simulating a given problem, ideally all possible solutions and outcomes should be included, however this is impossible to achieve. One cannot take every possible interaction made by a proton beam passing through a patient into consideration. However, an estimated average can be made given a large amount of random particle tracks used in simulation. This is called the law of large numbers [41].

Common for all Monte Carlo simulations is that a detector or a measurement instrument must be chosen, a way to keep the ”score”. For the simulations in this thesis the scoring option USRBIN was used. This is a method called “binning” where the particles are scored in a uniform spatial mesh that is independent of the geometry [42].

Before being able to start the simulation the DICOM files must be sorted. This was done using the sort_dicoms_impt.py script, creating a folder containing the DICOM files as well as material conversions. Furthermore, the Hounsfield units outside the patient was set to vacuum (-1024 HU) with the set_HU.py script.

Next the input file created for one of the treatment fields was opened in FLAIR and the CT images imported. Using the material definitions (eclipse_materials.inp) and calibration curves (eclipse_calibrationcurve.mat), a voxel file was made.

The FLUKA user routine fluscw is used to convert the fluence into a dose equivalent, by returning a multiplication factor for the fluences simulated [42]. The fluscw file was edited to carry out the necessary calculations for the different models and pO_2 levels. The α/β was set to 10 Gy and the model by Dahle et al. [6] was used for the OER calculations. For RBE calculations standard RBE1.1 and the Rørvik weighted RBE model [5] were used.

The Rørvik weighted RBE model is made to include a dependency on the full dose weighted LET spectrum, by using *rmax(L)*, a biological weight function based on in vitro cell data experiments, resulting in equation 5.2-5.3.

$$RBE_{max}(d(L),(\alpha/\beta)_x) = \int_0^{\infty} r_{max}(L,(\alpha/\beta)_x)d(L)\ dL \tag{5.2}$$

$$r_{max}(L,(\alpha/\beta)_x) = \begin{cases} 1+\frac{1\ Gy}{(\alpha/\beta)_x}(0.578(keV/\mu m)^{-1}L - 0.0808(keV/\mu m)^{-2}L^2 + 0.00564(keV/\mu m)^{-3}L^3 \\ \qquad -9.92\times10^{-5}(keV/\mu m)^{-4}L^4), L < 37.0\ keV\mu m^{-1} \\ 1+\frac{10.5\ Gy}{(\alpha/\beta)_x}, L \geq 37.0\ keV\mu m^{-1} \end{cases} \tag{5.3}$$

Where L is the LET and the remaining variables are the same as for equation 3.4-3.7. RBE_{min} was assumed constant and equal to 1 as other previous models have shown only slight deviations of β compared to β_x, resulting in equation 5.4.

$$RBE_{min} = 1 \tag{5.4}$$

RBE_{max} and RBE_{min} are then used in equation 3.7 to complete the RBE calculations. The Rørvik RBE weighted model and a constant RBE of 1.1 will be used throughout this thesis for comparison.

With the necessary alterations done to the fluscw file, the simulations were performed for all three fields with 100 000 primaries, 2 spawns and 5 cycles. The resulting bnn files were converted into a text file using ASCII (American Standard Code for Information Interchange) giving bnn.lis files. Before finally using convert_to_dicom.py to convert them into DICOM files. This resulted in dose distribution files for the physical and biological

RBE1.1 dose, dose averaged LET (LETd) as well as doses for Rørvik and RBE1.1 at 60 mmHg for normoxic tissue and at 10 mmHg, 7.5 mmHg and 5 mmHg for the different hypoxic thresholds.

Using Python, the combined dose volume histogram (DVH) for the whole PTV at the different pO_2 thresholds was plotted. This was done by combining the OER weighted dose to the hypoxic subregions with the normoxic dose to the surrounding PTV. The two doses were normalized by multiplying the doses with their respective volumes, adding them together and then dividing by the volume of the whole PTV.

5.3 Optimisation

The next step was to optimise the plan to overcome the radioresistance caused by hypoxia, using Eclipses' built-in optimiser. Firstly, three copies of the original plan were made, one for each of the hypoxic thresholds. The goal was to keep the original upper and lower dose objectives for the surrounding PTV, while increasing the objectives by multiplying the OER factor for the hypoxic subvolume. The divide between the surrounding PTV and hypoxic subvolume is abrupt. A margin was therefore created for each of the different hypoxic volumes for optimisation. This was to hopefully increase the achieved dose within the hypoxic volume and not underdosing close to the border.

The margins were created using the "margin for structure" function under contouring in Eclipse with the different hypoxic subvolumes as targets. A symmetrical margin of the smallest possible value of 0.1 cm was chosen. "Boolean operators" was used to remove any margin created that went outside the original PTV (see figure 5.4). It was also used to create a new surrounding PTV for the remaining volume of the original PTV.

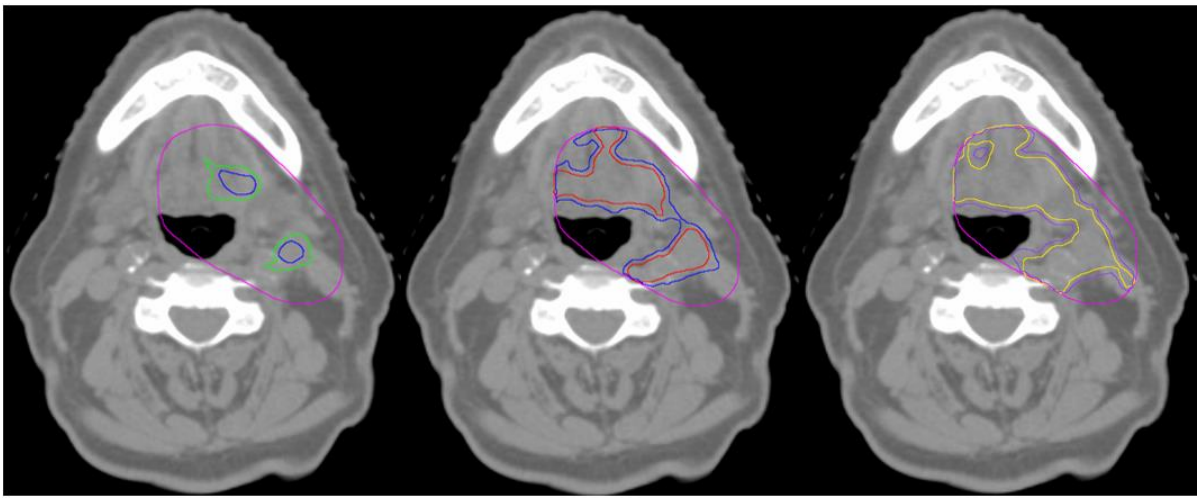

Figure 5.4: The resulting 0.1 cm margins created for each of the different hypoxic subvolumes. Left: The 5 mmHg subvolume in blue with the margin in green. Middle: The 7.5 mmHg subvolume in red with the margin in blue. Right: The 10 mmHg subvolume in yellow with the margin in purple. The PTV is outlined in pink in all the three pictures.

For optimisation the upper and lower dose objectives for all the surrounding PTV was set to 68.5 Gy (98%) and 71.5 Gy (102%). The different OER factors for the hypoxic thresholds were multiplied with these objectives giving upper and lower dose objectives for the hypoxic volumes. Thus modifying the dose levels to the hypoxic subvolumes for OER. Each limit in the Eclipse optimiser is given a weight to determine the importance of the objective and to prioritize them. All the limits to the hypoxic subvolumes and surrounding PTV were set to a priority of 100, making them of equal importance. This time the left parotid gland was not taken into consideration as to see what dose distribution could be achieved without having to account for it.

From there the different treatment plans were exported and the process described in chapter 5.2 repeated to allow further analysis. This resulted in dose distribution files for the physical and biological RBE1.1 dose, dose averaged LET as well as doses for Rørvik and RBE1.1 at 60 mmHg for normoxic tissue and at 10 mmHg, 7.5 mmHg and 5 mmHg for the different hypoxic thresholds.

5.4 Restricting dose to healty organs

When creating a treatment plan, several conciderations must be taken. Not only to achieve tumour control but also the quality of life after treatment. As mentioned in chapter 3.1, QUANTEC was created to have an overview of the tolerated doses of the different organs in the human body [22]. Depending on the organ and the consequences of overirradiation to that particular organ, the plan may be adapted to decrease the dose.

Table 5.3 shows the different organs and their corresponding dose limits that were considered in this thesis. The doses shown are the physical dose without any concideration of RBE. Furthermore the irradiation type for the data used to estimate the dose limits for brain stem, spinal cord, cochlea, parotid and larynx where 3-dimentional conformal radiotherapy [22]. They may therefore not be valid for IMRT let alone IMPT. This must be taken into consideration when comparing the different dose limits.

Table 5.3: The different organs at risk considered in this thesis. The dose limits are expressed in Gy or volume expressed in cc (cm^3) or percentage receiving that dose. Lastly are the potential consequence of exceeding the given constraints. Dose limits for brain stem, spinal cord, cochlea, parotid and larynx are from [22] and thyroid and mandible from [43].

Organ	Dose [Gy] or dose/volume parameters	Consequence
Brain stem	Dmax <64 D1-10cc ≤ 59	Permanent cranial neuropathy or necrosis
Spinal cord	Dmax =50	Myelopathy
Cochlea	Mean dose ≤45	Sensory neural hearing loss
Parotid	Mean dose <25 For combined parotid glands Mean dose <20 For single parotid gland	Long term parotid salivary function reduced to <25% of pre-RT level
Larynx	Dmax <66 Mean dose < 50 Mean dose <44 V50 <27%	Vocal dysfunction Aspiration Edema Edema
Thyroid	V30 <60% Mean <45	Hypothyroidism
Mandible	V50 <31-32% or <31 cc	Osteoradionecrosis

6. Results

6.1 Concequence of hypoxia in the original treatment plan

Included in all the DVH plots in chapter 6.1 and 6.3 is the DVH from Eclipse (unlike the rest which are the results of FLUKA MC simulations) for the orignal treatment plan without any hypoxic considerations. This Eclipse DVH has the correct prescribed dose and an optimal shape. This is included so that all the different treatment plans, both the original and OER optimised ones, have the same baseline for comparison. FLUKA recalculations does lead to less steeper dose curves comapared to Eclipse, resulting in an exaggerated "tail" at the end of curves.

The influence of tumour hypoxia of the original plan is shown in figure 6.1. The plot on the left is with a fixed RBE of 1.1, while the other is made using the Rørvik weighted RBE model. From these plots one can see an overall higher dose is given when the RBE1.1 model is applied. Both plots have similar shape for all the different pO_2 thresholds. The whole PTV receives a dose up to around 60 Gy(RBE), where it sharply drops creating a "shoulder". These drops are consistent with the size of the hypoxic subvolumes, and with the lower biological dose received in the hypoxic subvolumes, as can be seen in table 6.1.

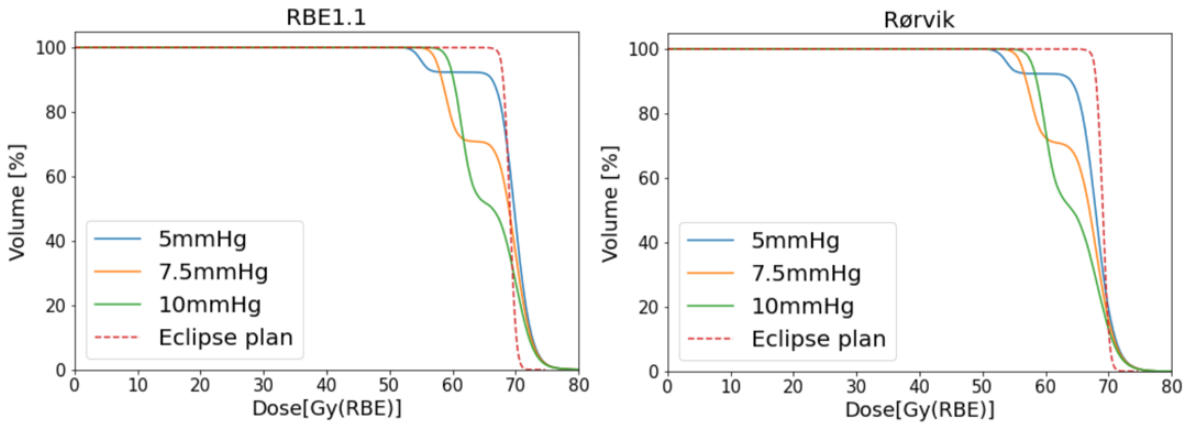

Figure 6.1: Shows the dose received per percentage of volume for the PTV with RBE1.1 and the Rørvik RBE model. Made combining the OER weighted dose to the hypoxic subvolumes with the dose to the surrounding PTV.

In figure 6.2 all the graphs in figure 6.1 are combined in one plot. Here one can clearly see that the doses have the same shape only increased for RBE1.1, which is shown with the solid lines.

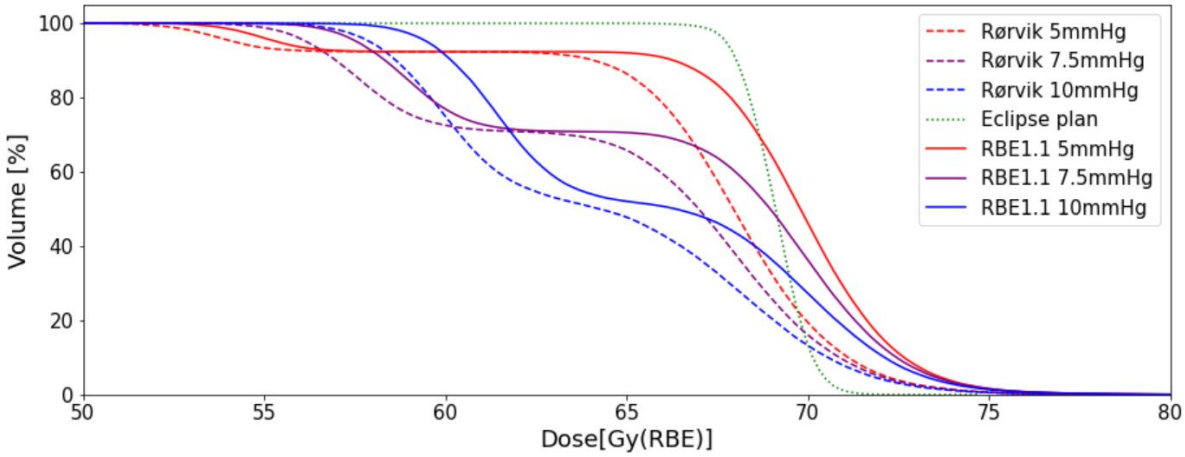

Figure 6.2: the combined DVHs for both RBE1.1 (solid) and Rørvik (dashed), with red, purple and blue for the 5 mmHg, 7.5 mmHg and 10 mmHg threshold. The green dotted line is the original Eclipse plan for comparison.

The mean, median and D95% biological doses to the different hypoxic subvolumes and their surrounding PTV are shown in table 6.1. Also the dose to the whole original PTV without any subvolumes or any hypoxic tissue considerations is included in the table. All the surrounding tissue doses, PTV5, PTV7.5 and PTV10 recives a nearly identical dose as the whole PTV without any subvolumes. This is to be expected as the tissue is normoxic, and no dose adaptations to the treatment have been included yet. For the hypoxic subvolumes, the OER adjusted biological doses are significantly lower than that of the corresponing surrounding PTVs. There is a the drastic difference of over 13 Gy(RBE) between PTV5 and PTV for both RBE models. Furtheremore, an increase in biological dose as the pO_2 increase can be seen.

Table 6.1: Mean, median and D95% dose received by the different structures with RBE1.1 and the Rørvik RBE model. 5 mmHg, 7.5 mmHg and 10 mmHg are the different hypoxic subvolumes while PTV5, PTV7.5 and PTV are the corresponding remainder of PTV. Furthermore, PTV is the whole original PTV without any subvolumes.

RBE1.1							
Structure	5 mmHg	PTV5	7.5 mmHg	PTV7.5	10 mmHg	PTV10	PTV
Mean [Gy(RBE)]	54.9	70.1	58.9	70.2	61.4	70.3	70.1
Median [Gy(RBE)]	54.9	70.0	58.9	70.1	61.4	70.2	70.0
D95% [Gy(RBE)]	53.1	66.8	56.6	66.8	58.9	66.7	66.9

Rørvik variable RBE model							
Structure	5 mmHg	PTV5	7.5 mmHg	PTV7.5	10 mmHg	PTV10	PTV
Mean [Gy(RBE)]	53.7	68.3	57.6	68.3	60.0	68.1	68.3
Median [Gy(RBE)]	53.7	68.2	57.6	68.2	60.0	68.1	68.2
D95% [Gy(RBE)]	51.7	64.7	55.1	64.6	57.3	65.1	64.8

In table 6.2 are the doses recived by the whole PTV when combining the biological dose to the hypoxic subvolume and the surrounding PTV. Furthermore, the dose to the whole original PTV is without any subvolumes or any hypoxic tissue considerations.

The lowest mean and median can be seen for PTV10 and increases for PTV7.5 and PTV5 as the hypoxic subvolume sizes decrease. Due to the small size of the 5 mmHg hypoxic volume, mean and median doses for PTV5 are very similar to that of the PTV. The D95% better reflect the low biological doses recived by the different hypoxic subvolumes. The PTV5 now have the lowest doses, increasing with almost equal increments of 2 Gy(RBE) towards PTV10.

Included in table 6.2 are also the maximum doses recived, where for RBE1.1 the maximum dose is 116% of the prescribed 70 Gy(RBE). Ideally one try to avoide a maximum dose over 107% or 74.9 Gy(RBE). However there is a drastic difference in the maximum dose from the FLUKA simulation and that of the Eclipse calculations, where the maximum dose is 74.6 Gy(RBE) or 107%. FLUKA recalculations tends to have higher maximum doses compared

to those calculated in Eclipse. Therefore when later looking at maximum dose for the OER adapted plans, they will be compared to 116% rather than 107% as they are also simulated in FLUKA.

Table 6.2: The mean, median and D95% dose of the combined hypoxic and surrounding PTV with RBE1.1 and the Rørvik RBE model. PTV5, PTV7.5 and PTV10 are the combined dose for the 5 mmHg, 7.5 mmHg and 10 mmHg hypoxic subvolumes and their corresponding remaining PTVs. Furthermore, PTV is the whole original PTV without any subvolumes.

	RBE1.1				**Rørvik variable RBE model**			
Structure	**PTV5**	**PTV7.5**	**PTV10**	**PTV**	**PTV5**	**PTV7.5**	**PTV10**	**PTV**
Mean [Gy(RBE)]	68.9	66.9	66.0	70.1	67.2	65.2	64.2	68.3
Median [Gy(RBE)]	69.8	69.0	66.3	70.0	67.9	67.0	64.2	68.2
D95% [Gy(RBE)]	55.4	57.6	59.5	66.9	54.2	56.2	57.9	64.8
Maximum [Gy(RBE)]	81.0	81.0	81.0	81.0	78.5	78.5	78.5	78.5

Figures 6.3-6.5 show the dose distribution in a single slice. Figure 6.3 shows the physical dose, showing a relativly even distribution, but with a few hotspots. Also in the same figure is the LETd distribution. In theory the LET increases along the path as the dose deposistion of protons reaches a peak near the end of the range.

This can be seen in figure 6.3. All three fields are placed on the left hand side of the patient (CT picture from the bottom up, therefore on the right side in the figure). The LETd starts low near the entry of the fields and gradually increase towards the middle. The hot spot in the middel left of the PTV, is where all the three fields overlap at the end of their range increasing the LETd.

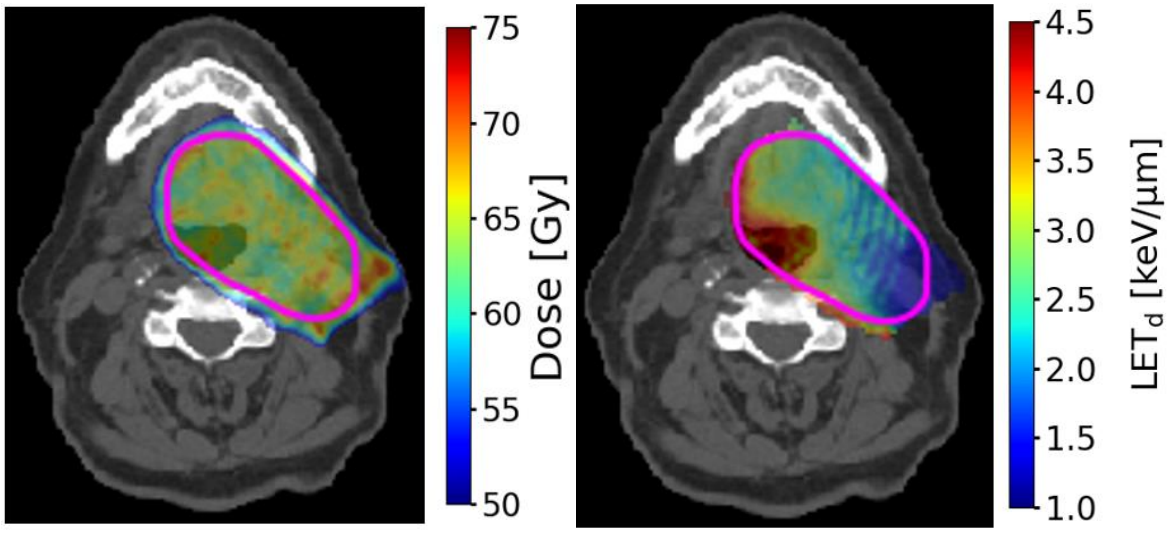

Figure 6.3: Left: the physical dose distribution. Right: LETd distribution. The pink circle is the original PTV.

Furthermore, in figure 6.4 is the comparison between the dose distribution for normoxic tissue for RBE1.1 and Rørvik. The largest dose difference is at the right slowly decreasing moving towards left, before the Rørvik RBE model has a higher dose than RBE1.1. The Rørvik model is dependent on the LET and, as discussed, the LET gradually increases along the path. The dose difference follows this LETd gradient.

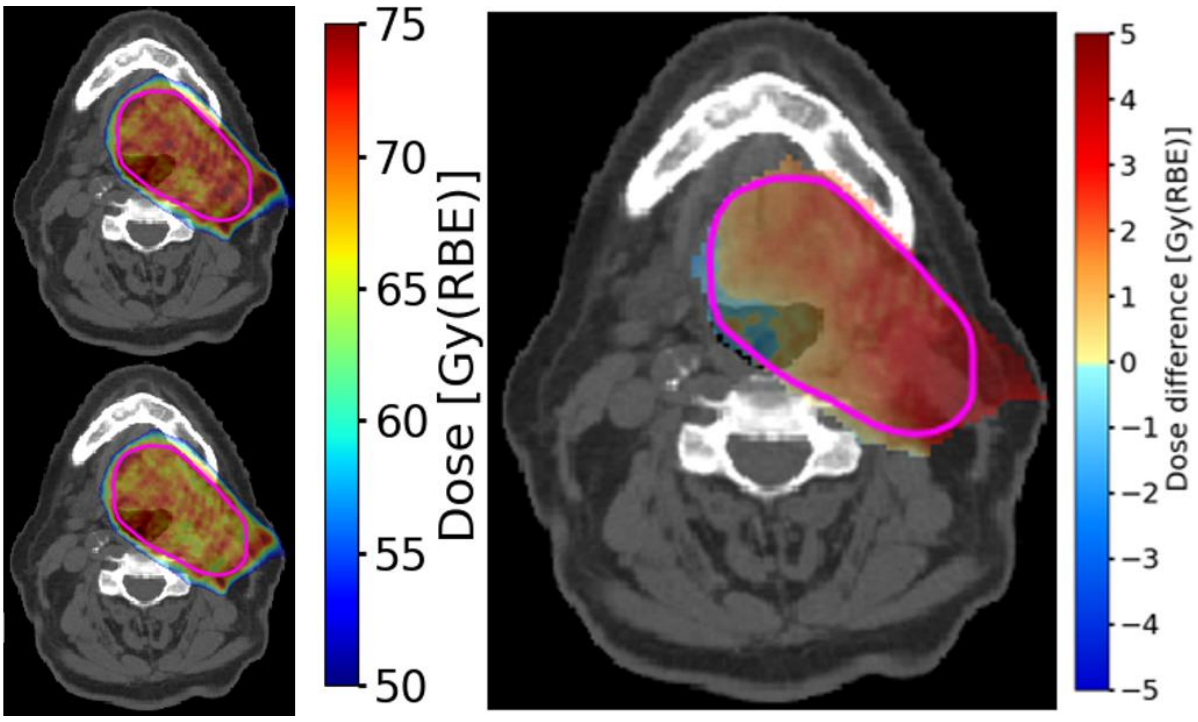

Figure 6.4: Top left: Biological dose for RBE1.1 at 60 mmHg. Bottom left: Biological dose for Rørvik without pO_2 consideration. Right: The dose difference between the two RBE models for normoxic tissue (RBE1.1 minus Rørvik). The pink circle in all the distributions is the PTV.

Figure 6.5 shows the combined dose distributions for RBE1.1 and Rørvik for the different hypoxic subvolumes. The hypoxic subvolumes have the OER adapted dose, while the surronding PTV have normoxic tissue doses. These images clearly show the drastic dose difference between the htpoxic and normoxic volumes. Moreover, it demonstrates the gradually decreasing dose from 10 mmHg volume to the 5 mmHg volume.

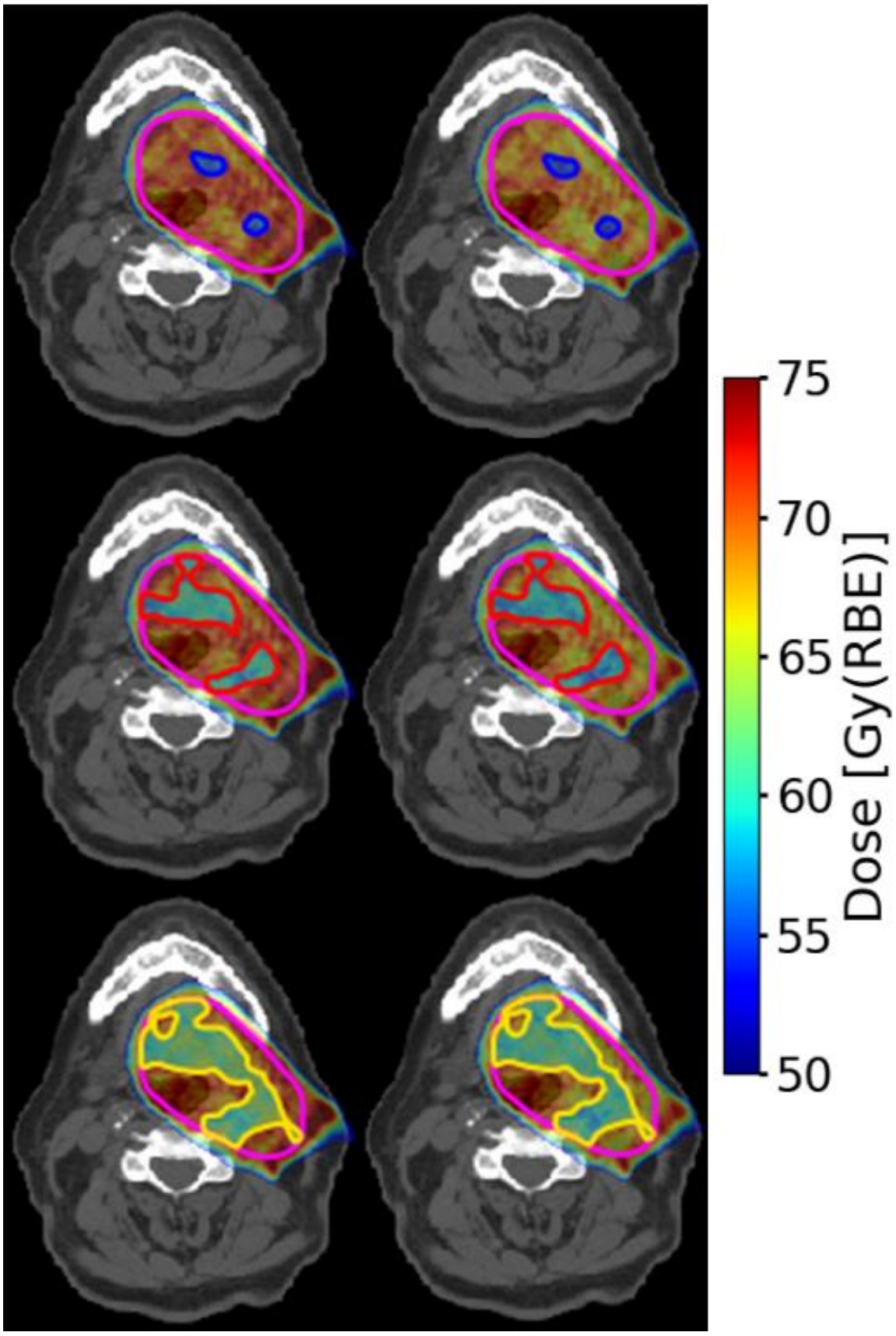

Figure 6.5: The combined dose distribution with RBE1.1 (left column) and the Rørvik RBE model (right column) for (from top to bottom) the 5 mmHg (blue), 7.5 mmHg (red) and 10 mmHg (yellow) thresholds. The pink outline is the PTV.

6.2 OER variables

To determine the upper and lower dose objectives, the OER factors for each hypoxic subvolume in figures 5.2 and 5.4 were derived from OER as a function of pO_2 calculated using equation 4.2-4.4. The different constants are $a_1 = 0.10$, $a_2 = 0.0010$, $a_3 = 0.010$, $a_4 = 0.0100$, $b_1 = 0.765$ and $b_2 = 0.273$ from Dahle et al. [6]. The LET was set to 2.6 KeV/µm as this is the mean of the original treatment plan (see table 6.3). This result is shown in figure 6.6, where the OER decreases as the pO_2 increases as expected from the theory chapter 4.2. The different pO_2 thresholds for the hypoxic subvolumes studied have an OER of 1.28, 1.19 and 1.14 for 5 mmHg, 7.5 mmHg and 10 mmHg respectively. This resulted in a lower and upper dose limit of 87.5 Gy and 91.4 Gy for 5 mmHg, 81.4 Gy and 84.9 Gy for 7.5 mmHg and 78.0 Gy and 81.4 Gy for 10 mmHg.

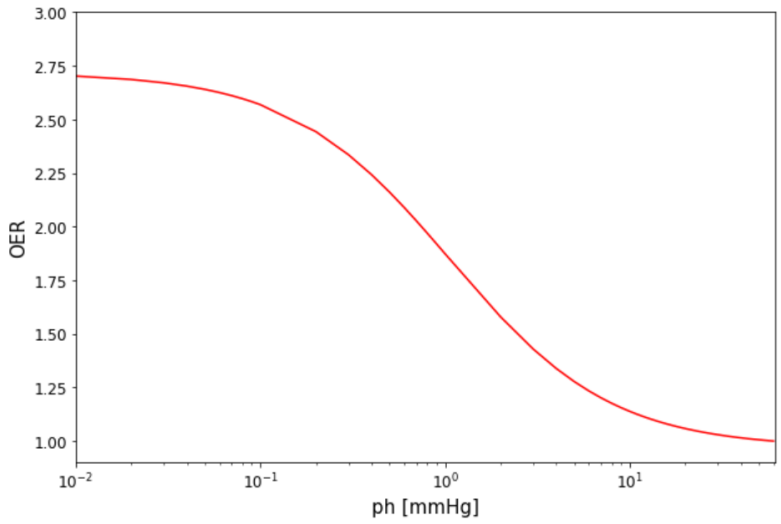

Figure 6.6: The OER dependency on pO_2 with 10% survival, LET_d = 2.6 KeV/µm and p_a= 60 mmHg.

6.3 OER optimised plan

As shown in figure 6.1 and 6.2 parts of the PTV, equivalent to the size of the hypoxic subvolumes, recives lower biological doses than desired. The dose with the constant RBE of 1.1 was therefore increased to the hypoxic subvolumes in Eclipse as described under methods, see chapter 5.3.

Figure 6.7 shows the physical dose for the new plans for the three different hypoxic thresholds. In each of the different treatment plans a significantly higher dose to the hypoxic subvolumes can be seen, as well as in the border areas between the normoxic and hypoxic regions. The mean physical dose has increased from around 64 Gy to 83.7 Gy, 76.3 Gy and 72.6 Gy for the 5 mmHg, 7.5 mmHg and 10 mmHg hypoxic subvolumes respectivly.

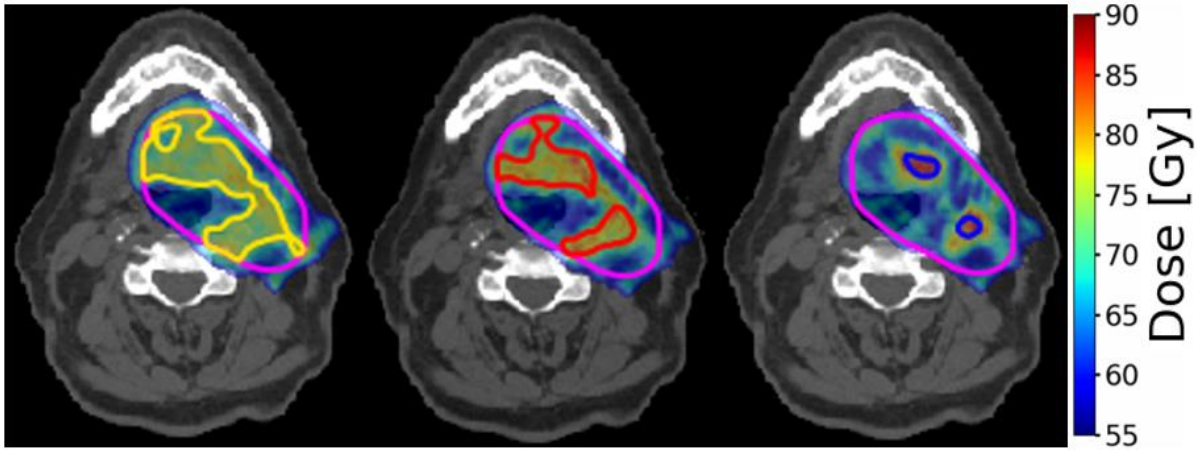

Figure 6.7: The physical dose distributions for the new optimized plans with increased dose to the hypoxic subvolumes. From left to right: 10 mmHg hypoxic subvolume (yellow) optimized plan, 7.5 mmHg hypoxic subvolume (red) optimized plan and the 5 mmHg hypoxic subvolume (blue) optimized plan. The pink outline is the PTV.

The LETd for the new optimized plans are shown in figure 6.8. The LETd distribution for the 10 mmHg dose plan is fairly similar to the original plan. For the 7.5 mmHg plan larger changes can be seen, some of which are inside the hypoxic subvolume. The largerst visible change in the LETd distribution is for the 5 mmHg plan. In this case there is a clear redistribution of the LETd, with higher values close to the right hypoxic subvolume as well as inside the left hypoxic subvolume.

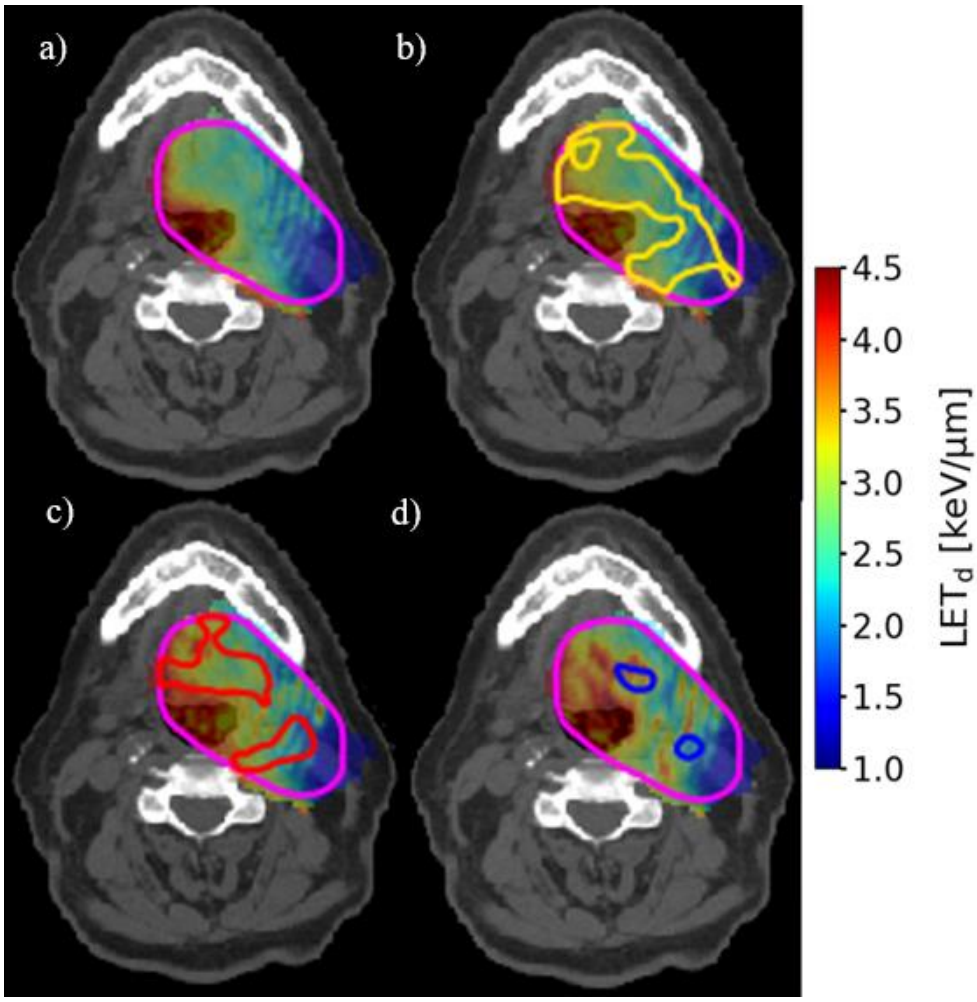

Figure 6.8: The dose averaged LET for the original plan (a) and new treatment plans (b) 10 mmHg, c) 7.5 mmHg, d) 5 mmHg). Yellow, red and blue is the 10 mmHg, 7.5 mmHg and 5 mmHg hypoxic subvolumes, whereas the pink outline is the PTV.

Table 6.3 includes the mean, minimum and maximum LETd for both the original and the new OER optimized plans. For both the mean and the minimum a gradual increase in the LETd can be seen from the original moving towards the 5 mmHg threshold plan. The LETd minimum and mean increases as the highest prescribed dose increase. For the maximum LETd, all the new OER adapted plans have lower values than the original with the 7.5 mmHg optimized plan at the lowest with 5.51 keV/µm.

Table 6.3: The mean, minimum and maximum of the dose averaged LET for the whole PTV for the original plan as well as the 5 mmHg, 7.5 mmHg and 10 mmHg OER optimized plans.

Dose averaged LET [keV/µm]				
Treatment plan	**Original**	**10 mmHg**	**7.5 mmHg**	**5 mmHg**
Mean	2.63	2.77	2.85	2.92
min	1.09	1.10	1.14	1.17
max	6.30	6.08	5.51	5.76

The combined DVHs for the new OER optimised plans are shown in figures 6.9, 6.11 and 6.13. For all the different hypoxic thresholds an improvement has been made as there are no longer a distinct “shoulder”. There are however varying degree of improvement.

Also in figures 6.10, 6.12 and 6.14 are the combined dose distributions for the different hypoxic thresholds. As before they are made combing the dose distribution for normoxic tissue for the surrounding PTV and the dose distrubutions for the different hypoxic thresholds inside the hypoxic subvolumes.

First the results for 5 mmHg RBE1.1 and Rørvik in figure 6.9 are discussed. The DVH curve for RBE1.1 has the best dose coverage of all the treatment plans. Here the new OER optimized plan and the Eclipse plan follow along for the initial curve as the volume drops from 100%. There is not an equally good coverage for Rørvik, however this is to be expected as Rørvik have lower overall RBE weighted dose. Moreover since the optimiser is in Eclipse where the RBE is set to 1.1, it is expected that the curve will be a better match for the same RBE.

The overall OER weighted dose for the new plans is higher for both RBE models, both compared to the Eclipse plan and the simulated original plan. However the gap between the original and the optimized curves is slightly larger for Rørvik then RBE1.1.

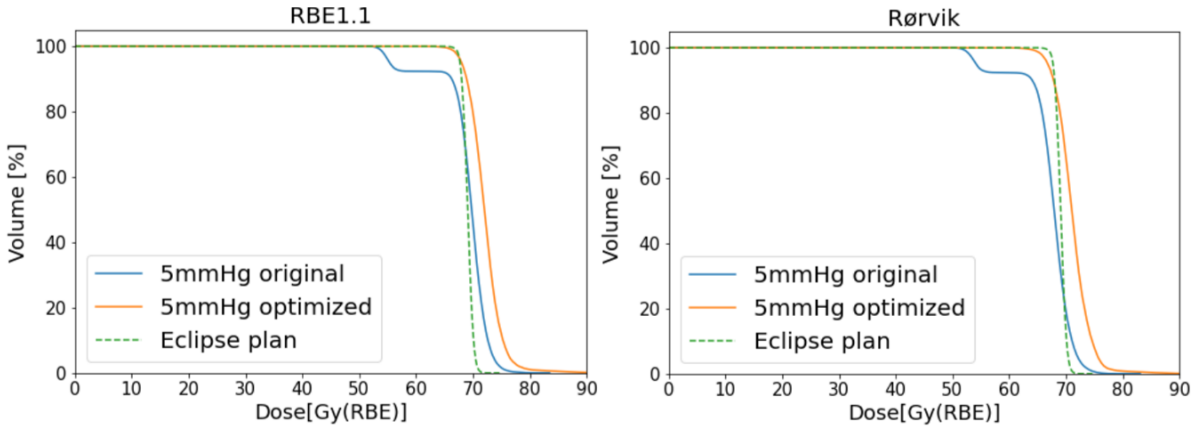

Figure 6.9: Combined DVHs plots for the original plan (orange), new OER adapted plan (blue) and Eclipse plan for comparison (green) with RBE 1.1 and the Rørvik RBE model.

Shown in figure 6.10 are the 5 mmHg RBE1.1 and Rørvik combined dose distribution for the hypoxic subvolumes and the surrounding PTV. The dose distributions only have small differences between them, mainly a slight increase in dose for the RBE1.1. This is expected from the similarity in the DVHs and the continously higher doses seen whenever RBE1.1 is used. There is a significant increase in dose at the border between the hypoxic subvolumes and the surrounding PTV. The shape of the area with increased dose roughly follows that of the margin used for optimisation seen in figure 5.4. The increase in dose is a concequense of these margins.

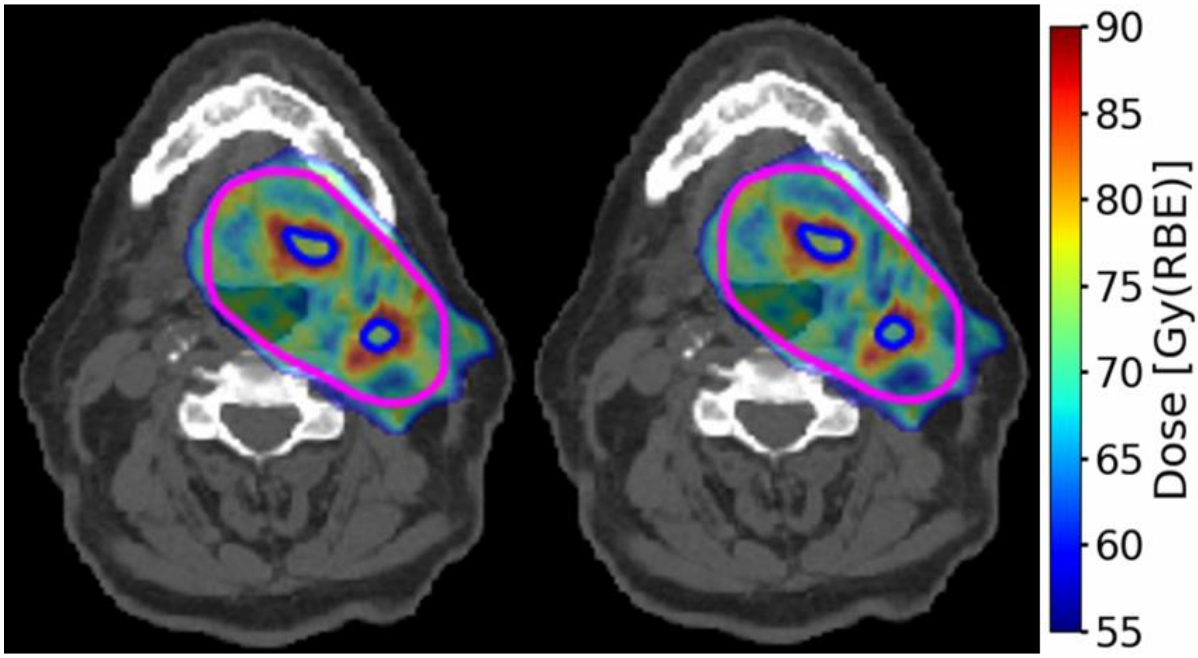

Figure 6.10: The dose distribution for the 5 mmHg optimized plan with RBE 1.1 (left) and the Rørvik RBE model (right). The blue outline is the 5 mmHg subvolume and the PTV outlined in pink.

Table 6.4 gives the mean, meadian and D95% for the hypoxic subvolume, surrounding PTV and the whole PTV including the OER adjusted dose to the hypoxic subvolume. Compared to the original plan, the dose to the hypoxic subvolume is significantly increased with over 17 Gy(RBE) for the mean and median and over 15 Gy(RBE) for the D95% for both RBE1.1 and the Rørvik RBE model. This could also be seen in the DVHs and dose distributions (figure 6.9-10). The median dose to the surroundig tissue is similar to the original plan, whereas the mean doses are increased and D95% are decreased. Looking at the maximum dose for the hypoxic region with RBE1.1 it is the same as that of the original plan with 116%. The surrounding normoxic tissue and the PTV as a whole however have a max dose of 143% or 27% higher than that of the original plan. The surronding PTV has therefore less dose coverage with more hot spots reciving higher doses. The hotspots are mainly the border regions as seen in the dose distribution.

Table 6.4: The mean, median and D95% dose for the new 5mmHg OER adapted plan for RBE1.1 and Rørvik RBE model. "5 mmHg" is the hypoxic subvolume made with a 5mmHg threshold, "PTV5" is the remaining PTV while "PTV" is the whole PTV with the combined dose of both volumes.

[Gy(RBE)]	**RBE1.1**			**Rørvik variable RBE model**		
Structure	**5 mmHg**	**PTV5**	**PTV**	**5 mmHg**	**PTV5**	**PTV**
Mean	72.1	72.3	72.3	71.2	70.7	70.8
Median	72.1	70.6	72.0	71.1	69.2	71.0
D95%	68.4	65.2	68.0	67.3	63.3	66.8
Maximum	81.2	100.3	100.3	80.4	98.8	98.8

Secondly, the DVHs for 7.5 mmHg optimized plan with RBE1.1 and Rørvik shown in figure 6.11 are discussed. Compared to the plots for 5 mmHg, they are less satisfactory, both in terms of dose coverage and the steepness of the curves.

In regards to the dose coverage it is still realativly well for RBE1.1. However for the Rørvik model, approxemetly 30% of the total volume recives a lower dose then desired. Furthermore, for both RBE1.1 and Rørvik, the tails of the curves are unsatisfactory, both in steepness and moreover the high dose values reached. For RBE1.1 approximately 8% of the

volume recives a dose of 80 Gy(RBE). Despite the overall lower dose for Rørvik, approximately 4% of the volume still recives 80 Gy(RBE) as well. A tail to this extent is not seen for either 5 mmHg or 10 mmHg.

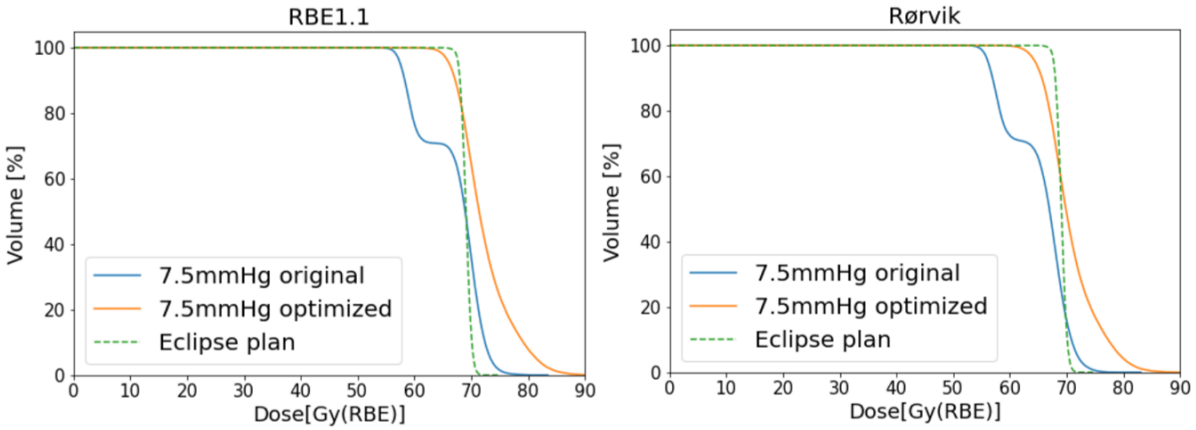

Figure 6.11: The DVHs for the 7.5 mmHg hypoxic threshold with RBE1.1 and the Rørvik RBE model. Includes the original plan (blue), the OER adapted plan (orange) and the Eclipse plan (green) for comparison.

The dose distributions in figure 6.12 show an overall good dose coverage and increased dose to the hypoxic subvolume. There is a significant hotspot forming a “bridge” between the hypoxic subvolumes. This is firstly because the two hypoxic subvolumes connect here in the following slices, leading to increased dose in the border bellow. Secondly, the extended margin applied to the hypoxic volume used for optimisation cover this area, as seen in figure 5.4.

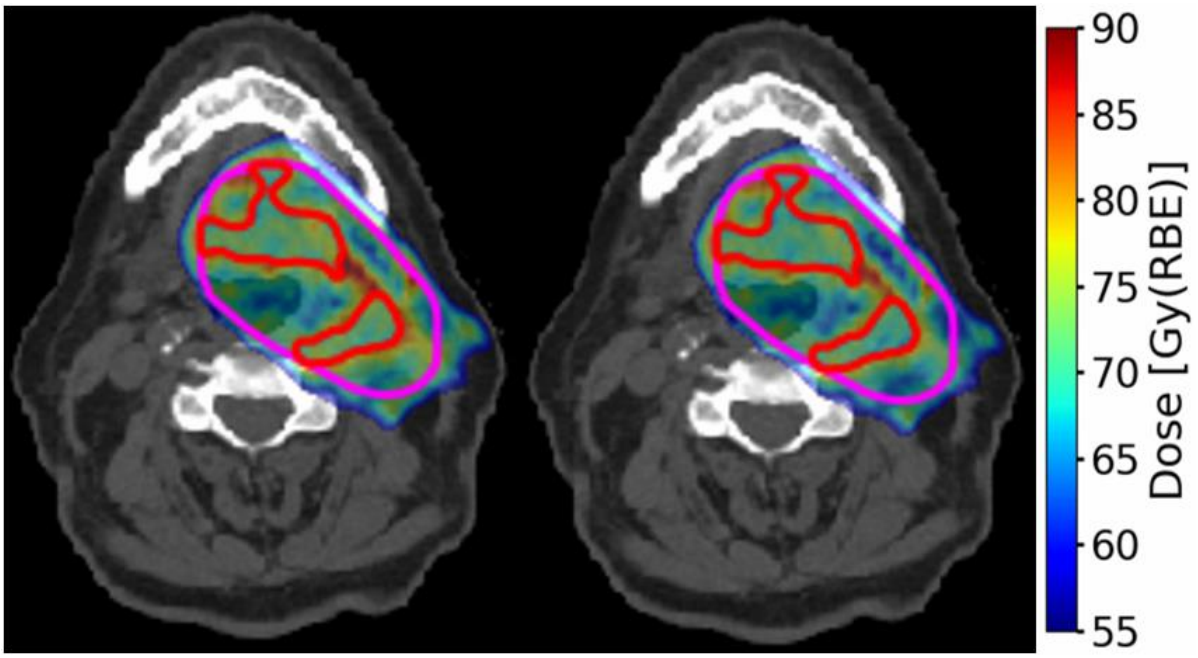

Figure 6.12: Shows the dose distribution for the 7.5 mmHg OER adapted plan with RBE1.1 and the Rørvik RBE model. The red outline is the 7.5 mmHg hypoxic subvolume and the PTV is outlined in pink.

The dose to the hypoxic subvolume in table 6.5 is close to ideal, with an approximetly 1 Gy(RBE) higher D95% compared to the 5 mmHg plan. However as before, the overall dose to the surrounding PTV is increased, while the dose coverage is decreased. To the PTV as a whole, the median and mean dose for Rørvik are close to optimial, whereas for RBE1.1 they are slightly high. Furthermore, the D95% slightly low for both. The maximum dose recived to the surronding and whole PTV is significantly reduced compared to the 10 mmHg OER optimised plan, especially for Rørvik. Moreover, comparing the prescribed dose of 70 Gy(RBE) to the maximum dose for RBE1.1 to the hypoxic volume and the surrounding PTV now give 114% and 135% doses. This is a slight decrease for the hypoxic volume, while it reflects the large decrease seen for the whole and surrounding PTV. The overall values for both RBE1.1 and Rørvik are promising, if it were not for the poor distribution shown in the DVHs.

Table 6.5: The mean, median and D95% dose for the 7.5 mmHg OER optimized plan with RBE1.1 and the Rørvik RBE model. “7.5 mmHg” is the hypoxic volume with a 7.5 mmHg threshold, “PTV7.5” is the remaining PTV and “PTV” is the two volumes combined.

[Gy(RBE)]	**RBE1.1**			**Rørvik variable RBE model**		
Structure	**7.5 mmHg**	**PTV7.5**	**PTV**	**7.5 mmHg**	**PTV7.5**	**PTV**
Mean	70.7	73.0	72.3	69.4	71.2	70.7
Median	70.6	72.2	71.4	69.3	70.4	69.9
D95%	67.2	65.9	66.2	65.6	64.1	64.5
Maximum	79.8	94.6	94.6	78.6	91.3	91.3

Lastly, the results for 10 mmHg RBE1.1 and Rørvik in figure 6.13 are discussed. The dose coverages are similar to those for 7.5 mmHg optimized plan. The steepness of the curves are still not ideal, however an improvement over 7.5 mmHg optimized plans’ long tails. The overall shape is fairly good, especially when compared to the 10 mmHg original plan.

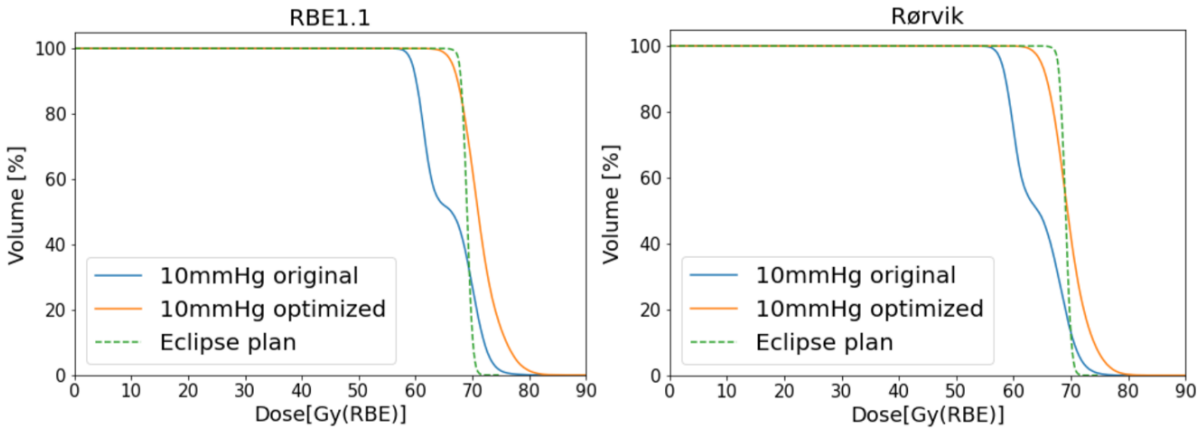

Figure 6.13: DVHs for the 10 mmHg threshold plans with RBE1.1 and the Rørvik RBE model. The original plan is in blue, the new OER optimized plan in orange and the Eclipse plan for comparison in green.

The corresponidng dose distributions are shown in figure 6.14. The Rørvik model distribution reflects the results from the DVH, with some underdosage spread troughout the surrounding PTV. Otherwise, for both RBE1.1 and Rørvik there are an even dose distribution for the whole PTV, with no apparent hot spots.

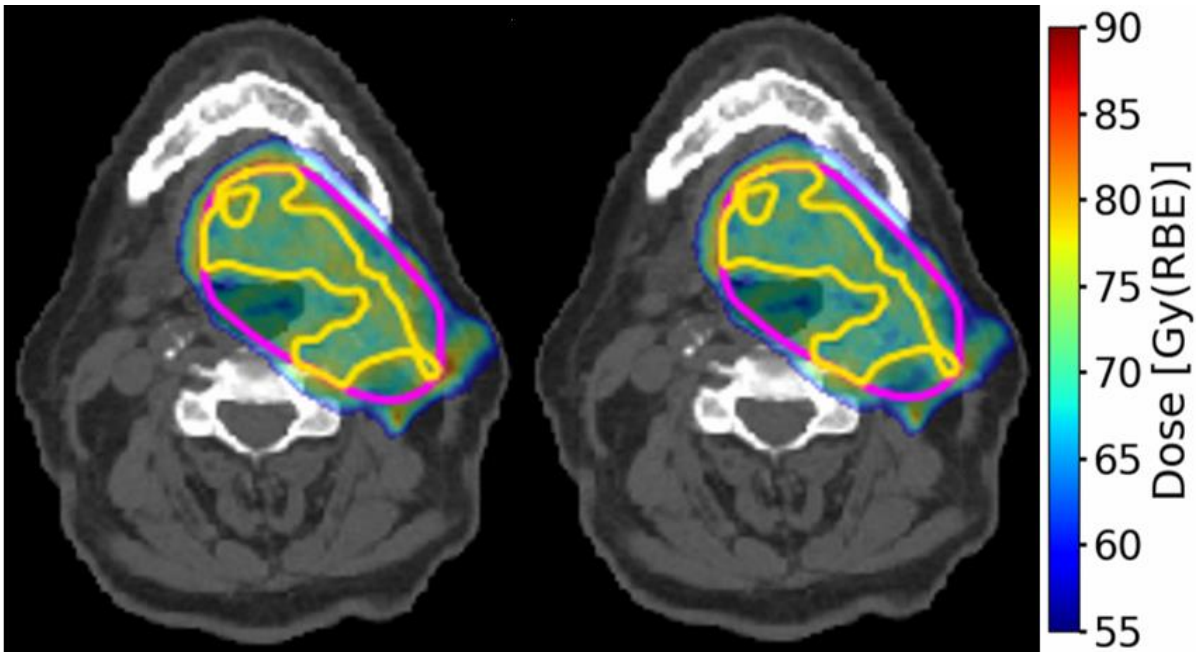

Figure 6.14: The dose distribution for the 10 mmHg OER optimized plan with RBE1.1 (left) and the Rørvik RBE model (right). The 10 mmHg hypoxic subvolume is outlined in yellow while the PTV is in pink.

The dose statistics for the 10 mmHg optimized plan can be seen in table 6.6. The D95% for both RBE1.1 and Rørvik show little variations, varying at most with 0.4 Gy(RBE). They are also similar to the D95% in the original plan for the whole PTV where there are no consideration towards hypoxia. This is also true for the mean and median for the hypoxic subvolume with both RBE models. However for RBE1.1 the surrounding PTV, and therefore the whole PTV, have slightly high values. The surrounding and whole PTV for Rørvik on the other hand have mean and median close to the prescribed dose of 70 Gy(RBE). The maximum doses recived for both RBE models are yet again decreased for all volumes, apart from the hypoxic subvolume for RBE1.1. It recives a 114% dose compared to the prescribed 70 Gy(RBE). Furthermore comparing the maximum dose to the prescribed for the whole and surrounding PTV results in 128%.

Table 6.6: The mean, median and D95% dose for the 10 mmHg OER optimized plan with RBE1.1 and the Rørvik RBE model. “10 mmHg” is the hypoxic volume with a 10 mmHg threshold, “PTV10” is the remaining PTV and “PTV” is the two volumes combined.

[Gy(RBE)]	**RBE1.1**			**Rørvik variable RBE model**		
Structure	**10 mmHg**	**PTV10**	**PTV**	**10 mmHg**	**PTV10**	**PTV**
Mean	70.1	72.6	71.4	68.5	70.8	69.7
Median	70.1	72.5	71.0	68.5	70.7	69.4
D95%	66.4	66.8	66.6	64.7	65.0	64.8
Maximum	79.9	89.3	89.3	77.4	86.2	86.2

Figure 6.15 shows the new optimized plan for all the different hypoxic threshold compared to one another. The overall best steepness and dose coverage for both RBE1.1 and Rørvik, are achieved for the 5 mmHg DVHs. However, all the DVHs for the OER optimised plans have a tail. This is likely because of the higher dose recived in the border between the hypoxic subvolume and the surronding PTV. As long as the hypoxic subvolumes are to recive a high enough dose to conteract the increased radioresistance, such a tail is likely unavoidable. Parts of the extended tails can however also be explained by using FLUKA for the recalculations, which tends to decrease the steepness of the curves.

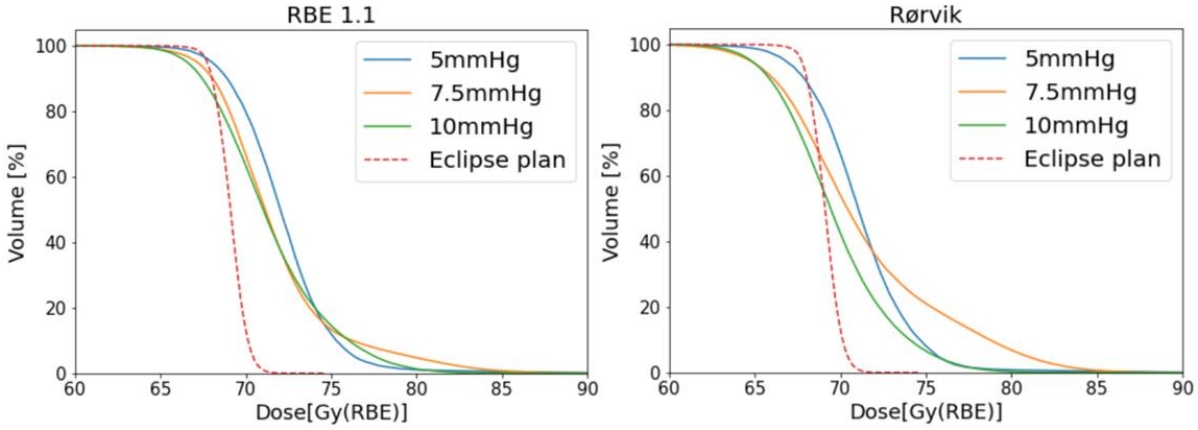

Figure 6.15: OER optimized plans for all the different hypoxic threshold, 5 mmHg (blue), 7.5 mmHg (orange) and 10 mmHg (green), as well as the Eclipse plan (red) for comparison.

6.4 Organs at risk

The QUANTEC dose limits shown in table 5.3 were compared to all four treatment plans used in this thesis. For nearly all organs the dose where either zero or well within the limits, with only slight variations in dose between the plans. The only partial exception is to the parotid glands.

The left parotid gland is partially within the PTV and as a consequence recives a high dose. Moreover the whole left parotid gland is between the PTV and all three fields, leading to parts of the beams traveling through the left parotid gland. Due to this, it recives a higher dose than those given in table 5.3. The mean dose to the right parotid gland is close to zero. The mean dose to the left and right parotid glands can be seen in table 6.7 and 6.8 for the four plans studied in this thesis. The dose is given for RBE1.1 calculated in Eclipse and FLUKA as well as with the Rørvik weighted RBE model with α/β equal to 10 Gy as well as 3 Gy.

Table 6.7: The mean dose to the left parotid gland for the original plan and the 5 mmHg, 7.5 mmHg and 10 mmHg OER optimized plans. The dose is given with RBE1.1 calculated in Eclipse and FLUKA and with the Rørvik weighted RBE model with α/β equal to 10 Gy and 3 Gy.

Mean dose to left parotid gland [Gy(RBE)]				
Treatment plan	**Original**	**5 mmHg**	**7.5 mmHg**	**10 mmHg**
Eclipse RBE1.1	38.2	35.9	36.6	41.8
FLUKA RBE1.1	39.8	37.6	38.4	43.7
Rørvik $\alpha/\beta = 10$	37.9	35.8	36.4	41.5
Rørvik $\alpha/\beta = 3$	39.9	37.7	38.3	43.6

Table 6.8: The mean dose to the right parotid gland for the original plan and the 5 mmHg, 7.5 mmHg and 10 mmHg OER optimized plans. The dose is given with RBE1.1 calculated in Eclipse and FLUKA and with the Rørvik weighted RBE model with α/β equal to 10 Gy and 3 Gy.

Mean dose to right parotid gland [Gy(RBE)]				
Treatment plan	**Original**	**5 mmHg**	**7.5 mmHg**	**10 mmHg**
Eclipse RBE1.1	0.001	0.001	0.001	0.001
FLUKA RBE1.1	0.001	0.01	0.01	0.01
Rørvik $\alpha/\beta = 10$	0.01	0.01	0.01	0.01
Rørvik $\alpha/\beta = 3$	0.02	0.02	0.02	0.02

7. Discussion

The motivation for this thesis was to simplify hypoxia cancer treatment planning by adapting correction methods for the increased radioresistance caused by hypoxia. As described previously, many of the approaches utilize a voxel-by-voxel method, leading to a range of pO_2 values be accounted for. By defining a whole volume to a single pO_2 value, the dose need only be adjusted to this value while still accounting for hypoxia in the tumour. Three different pO_2 thresholds with two different RBE models and corresponding OER adjusted dose have been explored in this thesis.

Comparing the shape of the DVH curves for the different pO_2 thresholds, the RBE1.1 DVHs are relatively similar as seen in figure 6.15. A larger difference can be seen with the Rørvik RBE model in the same figure. The shape for RBE1.1 and Rørvik for the 10 mmHg curves is almost identical however with a shift to lower biological doses. The similarities in shape can also be observed for the 5 mmHg optimised plan, with only a small increase in biological dose at the end of the curve for Rørvik, leading to an overlap with the 10 mmHg curve. For the 7.5 mmHg optimised plan however, the changes are more substantial. The varying RBE of the Rørvik model leads to an increase in biological dose for 50% of the tissue volume covered by the 7.5 mmHg Rørvik curve (see figure 6.11). This significant increase in dose is caused by a reduced steepness of the curve. The 7.5 mmHg is the only threshold where there is a significant difference in the slope between RBE1.1 and Rørvik.

The pO_2 thresholds explored have different strengths and weaknesses. The optimised plan for the 5 mmHg threshold showed the overall best dose coverage and steepness (figure 6.9, 6.10, 6.15 and table 6.4), however the small size of the 5 mmHg hypoxic volume may be an issue. As the 5 mmHg volume is 1/6 of the size of 10 mmHg (see table 5.2) a large amount of tissue deemed hypoxic by the other thresholds does not receive any increase in prescribed dose. This is partially solved by the elevated dose in the border area of the 5 mmHg hypoxic subvolume, however it may not be sufficient to overcome the radioresistance in the surrounding hypoxic tissue and achieve tumour control. Furthermore, comparing table 6.4 and table 6.1, the 5 mmHg hypoxic subvolume may receive a higher than necessary dose.

Since the 5 mmHg hypoxic subvolume was prescribed the highest dose, the dose modification should potentially be lowered.

Without looking at the results one might think a threshold of 7.5 mmHg would be ideal. The increase in prescribed dose for the 7.5 mmHg subvolume is in the middle of what is needed for the other two thresholds and the increased dose in the borders between the hypoxic volume and the surrounding PTV might be turned into something positive. This is because, the tissue deemed hypoxic at the 10 mmHg threshold may also receive an increase in dose, combating the increased radioresistance. However, the results for the 7.5 mmHg optimised plan, especially with the variable Rørvik RBE gives the poorest results of the optimised plans. Although the dose curves for RBE1.1 and Rørvik for 7.5 mmHg are quite different as seen in figure 6.15, they both have the same problem. The dose towards the end of the curves is considerably higher than for the 5 mmHg and 10 mmHg thresholds curves. This is especially true for the variable Rørvik RBE model. A possible explination could be the shape of the 7.5 mmHg subvolume. Perhaps it was challenging to conform to and the optimiser therefore was not able to achieve an equally optimal plan. It would be interesting to study if the results are reproducible for other HNC patients.

Lastly, is the 10 mmHg threshold. The 10 mmHg optimised plan has slightly lower dose coverage than the 7.5 mmHg optimised plan but has the advantage of a steeper dose curve with lower dose in the tail, as seen in figure 6.15. Moreover with 10 mmHg none of the tissue deemed hypoxic by any of the other pO_2 thresholds are ignored. However, the amount of increased dose needed to correct for the OER at 10 mmHg could be both an advantage and disadvantage. It may decrease the risk of side effects compared to the other thresholds as the dose is only increased by around 10 Gy(RBE) from the prescribed dose, whereas the OER adapted dose for the 5 mmHg thresholds increases with about 20 Gy(RBE). On the other hand, severely hypoxic tissue may be underdosed and might be unable to combat the increased radioresistance. When looking at the results for the 10 mmHg optimised plan with the Rørvik RBE model in figure 6.13, the biological dose is lower than for the Eclipse plan used for comparison for about 50% of the PTV. The lower dose coverage is troubling as it could lead to underdosage of the normoxic as well as hypoxic tissue and could therefore lead to lower tumour control. The same issue can also be seen for the 7.5 mmHg optimised plan

DVH with the Rørvik RBE model. In summary all the different pO_2 thresholds have their strength and weaknesses. Based on the results in this thesis alone the 5 mmHg threshold might be the best alternative.

The main OAR for this patient is the parotid glands. According to the QUANTEC guidelines [22] at least one of the parotid glands should be spared to a mean dose of less than 20 Gy. Eventhough the dose to the left parotid gland is well above 20 Gy(RBE), the mean dose to the right parotid is practically zero as can be seen in table 6.7 and 6.8. Acorrding to Deasy et al. [44] as long as one parotid is spared, the patient keeps the salivary function avoiding xerostima (dry mouth). Thus for this case, an increase in dose to the hypoxic regions could be concidered clinically and none of the plans where changed to lower the dose to the left parotid. However, as every patient is different the potential benefit must be considered against the possible side effects and impacts on each idividual patients quality of life.

There are some variations in the mean dose to the left parotid gland for the different treatment plans. The mean dose is reduced for the 5 mmHg and 7.5 mmHg OER optimized treatment plans compared to the original plan, whereas an increase could be seen for the 10 mmHg OER optimized treatment plan. The increase in mean dose is likely because of an overlap between the left parotid gland and the 10 mmHg hypoxic subvolume receiving a dose boost. Contrary to the 5 mmHg and 7.5 mmHg hypoxic subvolumes where there is no overlap.

Alterations in the LETd distribution varied for each of the different pO_2 thresholds, as seen in figure 6.8. The largest changes were seen for the 5 mmHg optimized plan, while the 10 mmHg optimised plan had only minor differences. This is most likely due to the size of the hypoxic volume. The 5 mmHg hypoxic volume is less than 1/6 of the 10 mmHg hypoxic volume, the change in dose and therefore also the change in LET is concentrated to that small volume. For the 10 mmHg optimised plan however, the hypoxic region is half of the total volume, leading to smaller changes in the original dose and LET distribution.

All the simulations for OER optimised plans have been done with the same field setup and weights to the hypoxic and surround tissue volumes. Alternative setups and weights have the

potential of improving the dose distribution. By comparing the DVHs of alternative setups and weights to the already simulated results in Eclipse, it could indicate if an improvement can be made. The upper and lower dose objective weights to our subvolumes were changed to different combinations of priorities. Furthermore, different field setups without changing the dose objective weight were evaluated. This included adding three identical fields targeting the hypoxic subvolume while the original fields targeted the surrounding PTV. Additionally, 18 fields were evenly spaced around the patient imitating an arc plan. There were no indications that different weights or the field setups tested would significantly improve the results.

As discussed previously all the DVHs show a tail of varying degree. With protons a higher dose conformity can be achieved compared to photons. However, even though it is highly improved, the dose cannot instantly increase or decrease. Therefore, if a highly elevated physical dose is to be delivered to the hypoxic volumes in accordance with the OER, an increase in dose outside the border is likely unavoidable. Alternatively, the optimisation can be done without margins to the hypoxic volume, having the decrease in dose inside the hypoxic volume, minimising the increase in dose to normoxic tumour tissue. However, doing such might risk underdosing the hypoxic tissue, resulting in lower tumour control than when using margins. A possible solution is to use carbon ions instead, as better dose conformity can be achieved with carbons compared to protons [45]. However as of present, no carbon therapy centres exist or are planned in Norway [46].

The method for FLUKA simulation and calculating RBE and OER weighted dose in this thesis is based on the method used in Dahle et al. [6] as described in chapter 4.4.3. Their method uses pO_2 voxel map to define the oxygen tension in the PTV. This was adapted and simplified to be pO_2 thresholds instead. Dose painting by numbers has the advantage of adjusting for each different voxels pO_2 level, however as seen in the Dahle et al. [6] it is not possible to achieve a perfect distribution, so parts are still underdosed. Furthermore, hypoxia is dynamic during the treatment curse [9]. Moreover, there could be uncertainties in the images themselves, both our understanding of hypoxia imaging properties of the tracer as well as conversion from signal to pO_2 value. By using pO_2 thresholds the plan may be more robust to these changes and inaccuracies. In addition, although Eclipse was used for the

original treatment planning in Dahle et al. [6], the optimiser used was not Eclipse. By using the inbuild optimiser in Eclipse, less additional equipment is required.

Another similar method to this thesis is presented by Toma-Dasu et al. [9] as described in chapter 4.4.1. Here the same uptake equation (eq. 5.1) is used to calculate the pO_2 values only with different constants as [^{18}F]FMISO is used as the tracer and not [^{18}F]EF5. Furthermore, 10 mmHg is used as a threshold to define the hypoxic volume and 60 mmHg is considered as normoxic, just as in this thesis. It is also similar to Dahle et al. [6] as a voxel-by-voxel dose modification is calculated. However, this study was done using IMRT and not protons. Consequently, no RBE is included in this model. It is well established that proton is superior to photons when it comes to dose conformity and tissue sparing. Moreover, a constant OER of 3 was used regardless of the pO_2 instead of a variable OER model such as in this thesis, which might lead to overdosage.

An alternative method is LET painting, which is compared to dose painting in Malinen et al. [3] as described in chapter 4.4.2. The study indicated that LET painting is not a standalone alternative method to combat hypoxia. The LET is likely to low for protons to achieve significant improvement with LET painting alone. A possible future study of trying to increase the LET to the hypoxic region defined by pO_2 thresholds using the method in this thesis would however be interesting.

In all the clinical studies mentioned in this thesis [10-15] delivery was done with photons, not protons. By using protons instead, dose conformity could be increased, increasing the chance to spare normal tissue and delivery of dose objectives. Furthermore, with the decreased OER and increased RBE and LET, the effects of hypoxia are minimized.

In the Welz et al. [10] clinical trial the hypoxic volume was defined using a hypoxia detection method based on tracer retention and perfusion. However, the physical dose to the hypoxic volume was not based on hypoxia related parameters, but simply increased with 10% of the prescribed dose.

Secondly, in Berwouts et al. [13] dose painting by numbers was studied. [^{18}F]FDG PET was used to define the hypoxic region, but instead of applying an uptake threshold correlating to the pO_2 levels, a cut-off for 50% of the uptake was set. Furthermore, was the dose

modification determined by dose and signal intensities, not by adapting for OER. As the hypoxic volume was manually outlined, the amount of work required for their method versus the method described in this thesis for defining the hypoxic region is likely equal. In Evensen et al. [11] the same equation as in in Berwouts et al. [13] is used to calculate the dose objective, only dose painting by contours instead. This again would likely be the same amount of work as OER adapting the dose.

The entire process for treatment planning adaptation explored in this thesis has the potential to be implemented clinically without any additional equipment (assuming access to [^{18}F]EF5 or uptake constants for equation 5.1 for a different tracer, and Eclipse treatment planning system or alternative program with similar functions). A predetermined constant for pO_2 threshold value to Bq/ml can be defined and the window level in the PET images adjusted accordingly. Then the dose can be adjusted for OER with a precalculated constant for the chosen pO_2 threshold. Lastly the plan can be optimised in Eclipse and adjusted before being ready to deliver.

When comparing this process to Evensen et al. [11] especially, it seems possible to implement the treatment planning adaptations in the clinic. Moreover, by both defining the hypoxic subvolume and dose escalation from the pO_2, tumour control could potentially improve.

Future work

Potential future endeavours may include:

- Combining the three different pO_2 thresholds by nesting them inside one another, adjusting the dose to each specific pO_2 threshold volume. This could create a more gradual decrease in physical dose.
- Further evaluating the method using TCP models
- Redistributing LET to the hypoxic subvolumes
- Evaluating the treatment planning adaptations preformed in this thesis on more patients
- Since several of the clinical trial uses [^{18}F]FDG as the PET tracer and there are [^{18}F]FDG PET images available for this patient, it could be interesting to use the method described in this thesis only with [^{18}F]FDG images instead for comparison.

8. Conclusion

In this thesis a method for determining the hypoxic regions using pO_2 thresholds for proton therapy in a HNC patient was developed. The dose was adjusted for RBE and each pO_2 threshold's OER. By executing FLUKA MC simulation the biological dose to the hypoxic regions could be studied. An overall lower biological dose to the hypoxic subvolumes was seen compared to the surrounding normoxic tissue. By increasing the dose objectives to the hypoxic regions with a calculated OER factor, the physical dose was successfully increased in the treatment plan for each hypoxic threshold. The biological doses achieved were close to the prescribed dose of 70 Gy(RBE) for all the hypoxic subvolumes. However, the biological doses to the surrounding normoxic tumour tissues were also increased. The doses received by the surrounding normal tissue and OARs were well within the limits set by QUANTEC except for the left parotid gland. Since xerostima can be avoided if one parotid gland receives a dose lower than 20 Gy and the dose to the right parotid was close to zero, the treatment plans were not adjusted. The overall best dose coverages for the OER optimised plans with both RBE1.1 and the Rørvik RBE model were seen for the 5 mmHg threshold. The method for treatment planning adaptions should be possible to replicate using Eclipse treatment planning system. The method successfully increased the biological dose for three pO_2 threshold defined hypoxic regions and has the potential to be implemented into clinical practice.

Bibliography

1. Mayo-Clinic. *Cancer treatment*. 2022 [cited 2022 07.06.]; Available from: https://www.mayoclinic.org/tests-procedures/cancer-treatment/about/pac-20393344.
2. Khan, F.M. and J.P. Gibbons, *Khan's the physics of radiation therapy*. Sixth edition. ed. Physics of radiation therapy. 2020, Philadelphia, Pennsylvania: Wolters Kluwer.
3. Malinen, E. and A. Sovik, *Dose or 'LET' painting--What is optimal in particle therapy of hypoxic tumors?* Acta Oncol, 2015. **54**(9): p. 1614-22.
4. Wikipedia. *Particle therapy*. 2022; Available from: https://en.wikipedia.org/wiki/Particle_therapy.
5. Rorvik, E., et al., *A phenomenological biological dose model for proton therapy based on linear energy transfer spectra.* Med Phys, 2017. **44**(6): p. 2586-2594.
6. Dahle, T.J., et al., *The FLUKA Monte Carlo code coupled with an OER model for biologically weighted dose calculations in proton therapy of hypoxic tumors.* Phys Med, 2020. **76**: p. 166-172.
7. Carreau, A., et al., *Why is the partial oxygen pressure of human tissues a crucial parameter? Small molecules and hypoxia.* J Cell Mol Med, 2011. **15**(6): p. 1239-53.
8. Bristow, R.G. and R.P. Hill, *Hypoxia and metabolism. Hypoxia, DNA repair and genetic instability.* Nat Rev Cancer, 2008. **8**(3): p. 180-92.
9. Toma-Dasu, I., et al., *Dose prescription and treatment planning based on FMISO-PET hypoxia.* Acta Oncol, 2012. **51**(2): p. 222-30.
10. Welz, S., et al., *Dose escalation to hypoxic subvolumes in head and neck cancer: A randomized phase II study using dynamic [(18)F]FMISO PET/CT.* Radiother Oncol, 2022. **171**: p. 30-36.
11. Evensen, M.E., et al., *Mucosa-sparing dose painting of head and neck cancer.* Acta Oncol, 2022. **61**(2): p. 141-145.
12. Olteanu, L.A., et al., *Comparative dosimetry of three-phase adaptive and non-adaptive dose-painting IMRT for head-and-neck cancer.* Radiother Oncol, 2014. **111**(3): p. 348-53.
13. Berwouts, D., et al., *Three-phase adaptive dose-painting-by-numbers for head-and-neck cancer: initial results of the phase I clinical trial.* Radiother Oncol, 2013. **107**(3): p. 310-6.
14. Cooke, S., et al., *OA02.05 Local, Regional and Pulmonary Failures in the Randomised PET-Boost Trial for NSCLC Patients.* Journal of Thoracic Oncology, 2021. **16**(3).
15. Duprez, F., et al., *Adaptive dose painting by numbers for head-and-neck cancer.* Int J Radiat Oncol Biol Phys, 2011. **80**(4): p. 1045-55.
16. Newhauser, W.D. and R. Zhang, *The physics of proton therapy.* Phys. Med. Biol, 2015. **60**(8): p. R155-R209.
17. Henley, E.M., H. Frauenfelder, and A. Garcia, *Subatomic physics*. 3rd ed. 2007, Hackensack, N.J: World Scientific.
18. Johnson, T.E. and H. Cember, *Introduction to health physics*. Fifth edition. ed. 2017, New York: McGraw-Hill Education.
19. Parisa, A. and M. Amir, *Proton Therapy in Neurosurgery: A Historical Review and Future Perspective Based on Currently Available New Generation Systems.* International Clinical Neuroscience Journal, 2016. **3**(2): p. 59-80.

20. Mayles, P., A. Nahum, and J.C. Rosenwald, *Handbook of Radiotherapy Physics: Theory and Practice*. 2007, Baton Rouge: Baton Rouge: CRC Press.
21. Leer, J.W.H., *What the clinician wants to know: radiation oncology perspective.* Cancer imaging : the official publication of the International Cancer Imaging Society, 2005. **5 Spec No A**(Spec No A): p. S1-S2.
22. Marks, L.B., et al., *Use of normal tissue complication probability models in the clinic.* Int J Radiat Oncol Biol Phys, 2010. **76**(3 Suppl): p. S10-9.
23. McMahon, S.J., *The linear quadratic model: usage, interpretation and challenges.* Phys. Med. Biol, 2018. **64**(1): p. 01TR01-01TR01.
24. Rorvik, E., et al., *Exploration and application of phenomenological RBE models for proton therapy.* Phys Med Biol, 2018. **63**(18): p. 185013.
25. Fleming, I.N., et al., *Imaging tumour hypoxia with positron emission tomography.* Br J Cancer, 2015. **112**(2): p. 238-50.
26. Silvoniemi, A., *Novel Aspects for Methodology and Utilization of PET/CT Imaging in Head and Neck Cancer*, in *Otorhinolaryngology*. 2018, University of Turku. p. 126.
27. Horsman, M.R., et al., *Imaging hypoxia to improve radiotherapy outcome.* Nat Rev Clin Oncol, 2012. **9**(12): p. 674-87.
28. Wenzl, T. and J.J. Wilkens, *Modelling of the oxygen enhancement ratio for ion beam radiation therapy.* Phys Med Biol, 2011. **56**(11): p. 3251-68.
29. Scifoni, E., et al., *Including oxygen enhancement ratio in ion beam treatment planning: model implementation and experimental verification.* Phys Med Biol, 2013. **58**(11): p. 3871-95.
30. Smith, N.B. and A. Webb, *Introduction to medical imaging : physics, engineering and clinical applications.* 2011.
31. Abdulla, S. *PET imaging*. 2021; Available from: https://www.radiologycafe.com/frcr-physics-notes/molecular-imaging/pet-imaging/.
32. Kerner, G.S., et al., *An exploratory study of volumetric analysis for assessing tumor response with (18)F-FAZA PET/CT in patients with advanced non-small-cell lung cancer (NSCLC).* EJNMMI Res, 2016. **6**(1): p. 33.
33. Storesund, A., *Hypoxia in Proton Therapy*. 2021.
34. Toma-Dasu, I., et al., *Therapy Optimization Based on Non-linear Uptake of PET Tracers vs Linear Dose Painting.* IFMBE Procceedings, 2009. **25**: p. 221-224.
35. Grüner, E.R., *Compendium PHYS212 Medical Physics and Technology.* 2012.
36. Dhawan, A., et al., *Tumour control probability in cancer stem cells hypothesis.* PLoS One, 2014. **9**(5): p. e96093-e96093.
37. Silvoniemi, A., et al., *Repeatability of tumour hypoxia imaging using [(18)F]EF5 PET/CT in head and neck cancer.* Eur J Nucl Med Mol Imaging, 2018. **45**(2): p. 161-169.
38. Varian, *Elevate your treatment planning with Eclipse.* 2020.
39. Nagarjuna, B., *Adaptive Proton Therapy in Head and Neck Cancer*, in *Proton Therapy*, J.F. Thomas and B.-J. Maryann, Editors. 2020, IntechOpen: Rijeka.
40. Vlachoudis, V., *Flair: A Powerful but User Friendly Graphical Interface for Fluka*. 2009.
41. Johansen, A., *Monte Carlo Methods.* 2010. **7**: p. 296-303.
42. Ferrari, A., et al., *FLUKA: A Multi-Particle Transport Code.* 2005.
43. Brodin, N.P. and W.A. Tome, *Revisiting the dose constraints for head and neck OARs in the current era of IMRT.* Oral Oncol, 2018. **86**: p. 8-18.

44. Deasy, J.O., et al., *Radiotherapy dose-volume effects on salivary gland function.* Int J Radiat Oncol Biol Phys, 2010. **76**(3 Suppl): p. S58-63.
45. Sheng, Y., et al., *SU-F-T-198: Dosimetric Comparison of Carbon and Proton Radiotherapy for Recurrent Nasopharynx Carcinoma.* Medical physics (Lancaster), 2016. **43**(6): p. 3507-3507.
46. Group, P.T.C.-O. *Particle therapy facilities in clinical operation*. 2022; Available from: https://www.ptcog.ch/index.php/facilities-in-operation.